

Master of Science Thesis

Lower leg design and contact sensing of quadruped robot



**Politecnico
di Torino**



by

Paolo Romeo

Under the supervision of

Prof. Stefano Paolo Pastorelli
Dr. Victor Barasuol
Dr. Matteo Villa

Department of Electronics and Telecommunications
Politecnico di Torino
Torino, Italia
December 2021

© 2021 Paolo Romeo. All rights reserved.

DECLARATION BY THE SCHOLAR

I certify that:

- The work contained in this thesis is original and has been done by me under the guidance of my supervisors.
- The work has not been submitted to any other Institute for any degree or diploma.
- I have followed the guidelines provided by the Institute in preparing the thesis.
- I have conformed to the norms and guidelines given in the Ethical Code of Conduct of the Institute.
- Whenever I have used materials (data, theory and text) from other sources, I have given due credit to them by citing them in the text of the thesis and giving their details in the reference section.
- The thesis has been checked by anti-plagiarism software.

Paolo Romeo

Acknowledgement

It is hard to express in just a few line my gratitude towards the people that allowed me to reach this milestone that is the ending of my student's life; I have never been very good at expressing deep emotions in words, but I will try my best.

I want to, first of all, thank Claudio Semini, head of the Dynamic Legged Systems lab, for the opportunities he provided me, and the trust he put into me as I returned to the DLS lab for the second time.

I want to thank my supervisor prof. Pastorelli, your point of view always proved to be extremely valuable throughout the progress of the thesis.

I want to thank my supervisor Dr. Victor Barasuol, you taught me more on a human and professional level than you can ever imagine, and your lessons will remain impressed for years to come.

I want to thank my supervisor Dr. Matteo Villa, you were there for me every time I needed, pushing me to improve myself and being by my side when I could not find a way out.

I want to thank my Mechatronics colleagues at Politecnico di Torino, we managed to bond even in these challenging times, and you managed not to make me feel lonely even during multiple months of isolation.

I want to thank Laura, I would not be here without you and you know it, I will always be grateful for what you have done for me, and this achievement is especially dedicated to you.

I want to thank Antonio and Paola, you pushed me to overcome my limits and boundaries, I would not be who I am had I not met you.

And of course, I want to thank my parents, my family, to which I owe everything; you allowed me to experience another side of the world at an age that many Italian parents would still call "baby age", to have the freedom to find myself and to make mistakes, judging but not condemning me for what I am: 8 years after this is the minimum that I can do to thank you.

And last, I want to dedicate this to Giorgio and Lens, I have lost you in the last year without even being able to say goodbye, and I am still trying to cope with the grief. The world is not the same without you, and I miss you everyday.

Place: Istituto Italiano di Tecnologia , Genova

Date: December 9, 2021

Paolo Romeo

Abstract

Quadruped robots are ground mobile platforms with great capabilities to navigate on challenging surfaces, like on natural ground and unstructured environments. The key element behind such great capabilities is the level of adaptation that each single leg can provide with respect to the terrain surfaces and obstacle sizes. In this perspective, an effective leg design exploits as much as possible the range of motion of every joint to allow the robot torso to reach extreme postures during the navigation. During the locomotion, the lower link of a leg (the shin) is the robot link that has higher chances to make undesired contacts with the environment. Undesired contacts (or collisions) at the shin are dangerous and can make the robot get stuck or even fall, therefore, the design of the lower leg is directly associated to the robot limitations when navigating over rough terrain, for example, on rocks or stairs. In this thesis, we propose a study to aid the process of designing the new lower leg specifically for the task of stairs climbing, both for a generic quadruped robot, and for the hydraulic quadruped robot HyQReal. The thesis then tackles the mechanical design of the new foot of the HyQReal robot, studying new shapes, the addition of a contact sensor embedded in the foot, and the interface with the robot hardware. The choice of the sensor was aided by a model which, given certain weights to each of the benchmarks, returns the most promising sensor technology. Once the sensor has been assessed, it is first validated through numerical simulations performed using the Ansys software. Subsequently, a prototype is made and the performance of the new foot is evaluated.

Keywords: Quadruped robot design, Locomotion, Additive Manufacturing, Force Sensing Technology, Structural Analysis, Computer-Aided Design, Shape Optimization

List of Figures

1.1	Picture of HyQReal with labels indicating the key components [1].	2
1.2	System overview and main specifications for the robot HyQReal [1]	3
1.3	3D rendering of the ISA, developed by Moog in collaboration with the DLS lab [1].	3
2.1	Prismatic Leg topology [2]	12
2.2	Articulated legs types [3]	13
2.3	HyQ articulated leg [4]	14
2.4	HyQ2Max [5]	15
2.5	Articulated Leg topology [2]	16
2.6	Redundant Articulated Leg Topology [2]	17
3.1	Perception Loop [6].	22
3.2	OptoForce sensor, image courtesy of OptoForce Ltd.	25
3.3	Pressure measurement techniques, comprising absolute, gauge and differential measuring methodologies [7]	26
3.4	Bridge-based pressure sensor [8].	28
3.5	Capacitive pressure sensor [7].	29
3.6	Piezoelectric pressure sensor [9].	29
4.1	Cross section of the foot, as currently used in the robot HyQReal	33
4.2	Cross section of the first design of the new foot, comprising a spherical control volume and an unchanged pin.	34
4.3	Cross section of the second design of the new foot, comprising a toroidal control volume and a first attempt at redesigning the pin.	34
4.4	Cross section of the refined "smile" design	35
4.5	Preliminary test model	36
4.6	Zero load; no deformation.	37
4.7	50N normal load; -10% Δ Volume	37
4.8	250N normal load; chamber sealed.	37
4.9	Half cross section of one of the discarded designs.	37
4.10	Alternative version of the foot cross section	38
4.11	Alternative version of the foot, 3D	38
4.12	3D cross section of the foot, used as prototype for the experimental phase.	39
4.13	STL export of the 3D deformed model.	40
4.14	Reverse-engineering technique end result.	40
4.15	Cross section of the foot prototype.	40
4.16	No load applied, undeformed shape.	41

4.17	50N load applied; -10% Δ Volume.	41
4.18	100N load, chamber sealed and -20% Δ Volume.	41
4.19	50N load applied at 45°; -10% Δ Volume.	41
4.20	100N load applied at 45°; -18% Δ Volume.	41
4.21	250N load applied at 45°; -22% Δ Volume.	41
4.22	Cross section of the alternative proposed foot design.	42
5.1	Structure of the code	49
5.2	Script usage: generic leg output	56
5.3	Highlight of the shin bending, indicated by the blue arrow.	57
5.4	Result of the analysis: best shape for generic quadruped	58
5.5	Script output display of successful trials, for a generic leg configuration	59
5.6	Script output display of successful trials, after leg shape was optimized	60
5.7	Current lower leg version of the robot HyQReal.	60
5.8	Proposed design of the lower leg for the robot HyQReal.	60
6.1	Highlight of the sensor chamber, encapsulated in epoxy resin	64
6.2	First prototype of the foot assembly	65
6.3	Schematics for simultaneous read	66
6.4	Picture taken during the preliminary dead volume test of the sensor	66
6.5	First prototype dynamic behaviour as load is applied	67
6.6	Second prototype dynamic behaviour as load is applied	67
6.7	0.25 Hz triangular wave, data from force plate (orange) and pressure sensor (blue)	68
6.8	0.50 Hz triangular wave, data from force plate (orange) and pressure sensor (blue)	69
6.9	1.00 Hz triangular wave, data from force plate (orange) and pressure sensor (blue)	69
6.10	2.00 Hz triangular wave, data from force plate (orange) and pressure sensor (blue)	69
6.11	5.00 Hz triangular wave, data from force plate (orange) and pressure sensor (blue)	70
6.12	Experimental setup	71
6.13	Raw data from pressure sensor at high frequency vibrations	72
6.14	Stress test results, in blue beginning, in orange after one hour. Graphs superimposed a posteriori	73

List of Tables

2.1	The weight, payload-to-weight ratio, and maximum speed of significant quadruped robots in recent years [10].	11
3.1	Force/Contact sensors parameters of relevance considered in the analysis	30
3.2	Results of the analysis aimed at choosing the most appropriate force/contact sensor. The highest the total score, the better.	30
6.1	Experimental results: response time and gain	70
6.2	Experimental results: vibration effect on pressure reading.	71

Abbreviations

IIT	Istituto Italiano di Tecnologia
DLS	Dynamic Legged Systems
HyQ	Hydraulic Quadruped
HPU	Hydraulic Power Unit
ISA	Integrated Smart Actuator
KFE	Knee Flexion Extension
HFE	Hip Flexion Extension
HAA	Hip Abduction Adduction
DOF	Degree of Freedom
SIL	Safety Integrity Level
SEA	Series Elastic Actuators
CAD	Computer Aided Design
GUI	Graphic User Interface
FK	Forward Kinematics
IK	Inverse Kinematics
CoP	Center of Pressure
CoM	Center of Mass
ZMP	Zero Moment Point
FSR	Force Sensing Resistors
STL	Standard Triangle Language

Contents

Declaration	iii
Acknowledgement	v
Abstract	vii
List of Figures	ix
List of Tables	xi
List of Abbreviations	xiii
1 Introduction	1
1.1 HyQReal	2
1.1.1 Integrated Smart Actuator (ISA)	3
1.2 Stair Climbing	4
1.3 Contact Sensing	4
1.4 Dynamics of Legged Locomotion	6
1.5 Shin Shape Optimization	7
1.6 Contribution	7
2 Background	9
2.1 Leg Design	10
2.1.1 Prismatic Leg	11
2.1.2 Articulated Leg	12
2.1.3 Redundant Articulated Leg	15
2.2 Contact Sensing Technologies	17
3 Sensors	19
3.1 Introduction	20
3.1.1 Perception	21
3.1.2 Estimation	22
3.2 Choice of Sensor	23
3.2.1 Snap-Action Switches	24
3.2.2 Load Cell	24
3.2.3 Force Sensitive Resistors	24
3.2.4 OptoForce	25
3.2.5 Pressure Sensors	26

3.2.6	Pressure Measurement Methods	28
3.3	Sensor choice for HyQReal	29
4	Mechanical Design	31
4.1	Preamble	32
4.2	Foot Design	32
4.2.1	Choice of Materials	32
4.2.2	3D CAD Design	32
4.2.3	Third Design: Smile	35
4.3	Numerical Analyses: Ansys	36
4.3.1	STL export and volume definition	39
4.3.2	Validation of design and prototyping	39
4.4	Alternative foot design	41
4.5	Shin Design	43
5	Locomotion and Coding	45
5.1	Motivation	46
5.1.1	Workspace	47
5.2	Stair Climbing	47
5.3	Contact Awareness	47
5.4	Code Development	48
5.4.1	Input Definition	49
5.4.2	Kinematic Assessment	52
5.4.3	Output Function	55
5.5	Usage: Shin Shape Optimization for a generic Quadruped	55
5.6	Usage: Shin Shape Optimization	56
6	Experiments	61
6.1	List of Materials	62
6.2	Foot Prototyping	63
6.3	Data Collection	64
6.4	Sensor Testing	65
6.5	Force Plate Calibration and Prototype Preliminary Tests	65
6.5.1	Troubleshooting	67
6.6	Foot Testing	68
6.7	Vibration Effect on Sensor	70
6.8	Stress Test	72
7	Conclusions and Future Works	75
7.1	Conclusions	75
7.2	Future Works	76
	References	77

CHAPTER 1

Introduction

Chapter 1 is devoted to assessing the principal aspects and motivations that led to the elaboration of this work, it also intends to illustrate its main contributions. For this reason, we provide an introduction that gives an overview of the state of the art in legged locomotion, force and contact sensing technology, and the most recent developments and experimental results. It is then presented what are the criticalities of the current way in which contact with the ground is sensed in the robot HyQReal, and what the new design aims to achieve. It will be also assessed the rationale followed in optimizing the shape of the lower leg to improve reachability during stair climbing, which is currently one of the most compelling applications of legged robotics, but at the same time one of the most challenging to address and perform without incurring in critical (and dangerous) failures. Finally, it will be provided an analysis in the chapter 5 - Locomotion and Coding -, where it will be addressed the list of benefits that would be brought by having a sensed foot. In the last section of this chapter are reported the foremost contributions that the thesis wants to give with the development of the new robots being developed at the Dynamic Legged Systems (DLS) lab. The thesis was proposed and developed at IIT, standing for Istituto Italiano di Tecnologia, a scientific research centre based in Genoa (Italy, EU) with research lines in the field of robotics, artificial intelligence, smart materials, computer vision and neuroscience.

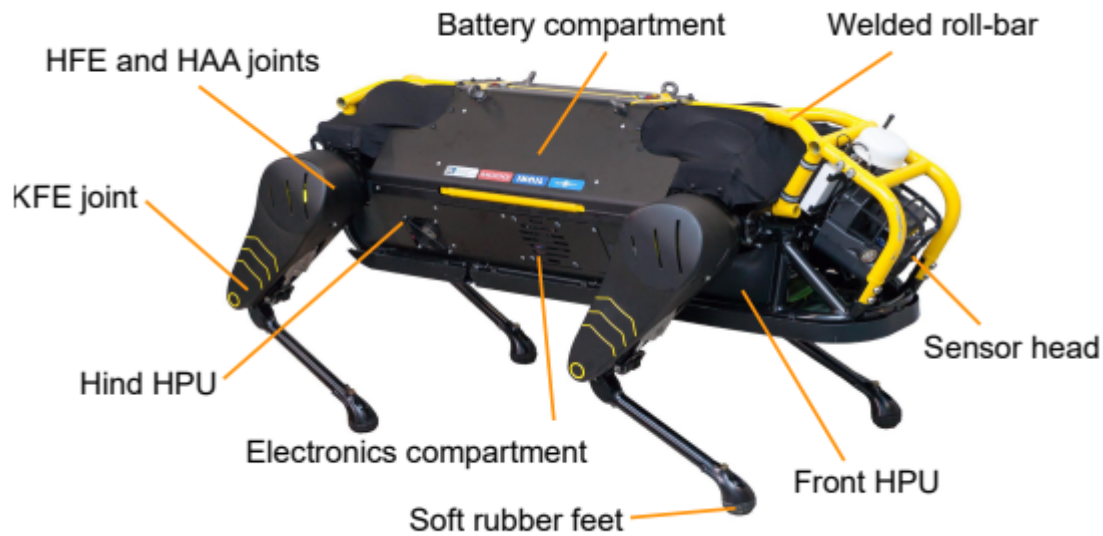


Figure 1.1: Picture of HyQReal with labels indicating the key components [1].

1.1 HyQReal

HyQReal [1] is the most recent version of IIT’s hydraulic quadruped robot series HyQ, and it is the result of a collaborative effort between IIT’s Dynamic Legged Systems Lab and its industrial partner Moog Inc., a world leader in reliable, high-performance actuation systems for aerospace and motorsport. Over the last 10 years, HyQ [11] has shown a wide repertoire of indoor/outdoor capabilities, from running and jumping to reflexes and carefully planned and unplanned walking over rough terrain. Its successor HyQ2Max was designed to be more rugged, with the added capability to perform self-righting maneuvers. While these versions are still used for state of the art research into rough terrain locomotion, they both lack power autonomy. This point was addressed in the third version of this robot - HyQReal - by integrating within the torso a full hydraulic power system (HPU) with Lithium Polymer (LiPo) battery. The robot parts that were custom designed are mainly made of a high strength aluminum alloy and stainless steel. A hollow aluminum spine ensures torsional rigidity, connecting the front and back legs points of contact. The robot has a layer of protection given by a roll cage, which acts as a rib cage with the goal of protecting the battery, the hydraulics, and the electronics from impacts. A skin made of Kevlar and glass fiber enhances the protection of the robot. Spherical rubber feet (with varying hardness based on the version) increase the traction between the feet and the ground.

The abbreviations have the following meaning: Hip Abduction Adduction (HAA), Hip Flexion Extension (HFE), Knee Flexion Extension (KFE) [1].

1.1 HyQReal

dimensions	1.3 m x 0.67 m x 0.9 m (LxWxH)
distance left/right HAA	0.278 m from axis to axis
distance front/hind HFE	0.887 m from axis to axis
link lengths	hip (HAA-HFE): 0.117 m upper leg (HFE-KFE): 0.36 m lower leg (KFE-foot): 0.38 m
weight (approximately)	130 kg (onboard hydraulics and battery)
active DOF	12
HAA actuators	double-vane rotary hydraulic actuators
HFE actuators	double-vane rotary hydraulic actuators
KFE actuators	asymm. hyd. cylinders & four-bar linkage
joint motion range	60° (HAA), 110° (HFE), 133° (KFE)
max. torque [HAA]	165 Nm (constant torque at 20 MPa)
max. torque [HFE]	270 Nm (constant torque at 20 MPa)
max. torque [KFE]	240 Nm (peak torque at 20 MPa)
position sensors	absolute position 19 Bit in all joints
torque/load sensors	torque (HAA, HFE), loadcell (KFE)
onboard computer	Intel core i7 with real-time Linux
joint controller rate	torque (5 kHz) & position (1 kHz, EtherCAT)

Figure 1.2: System overview and main specifications for the robot HyQReal [1]

1.1.1 Integrated Smart Actuator (ISA)

ISA stands for Integrated Smart Actuator, developed by Moog. They are part of the family of lightweight hydraulic actuators, and they integrate servovalves, sensors, control electronics, and bus communications through CANbus and EtherCAT. They are specifically designed for mobile robotic applications, requiring extremely high power density. As everything is integrated in an SLS 3D printed metal body, the weight is kept as low as possible, the power to weight ratio of the ISA is among the highest in the market. Other key features of the ISA include a highly advanced control structure, a real time high speed digital interface, integral position, force and pressure control, a Safety Integrity Level (SIL) 2, as per IEC Standards, configurable and easily adjustable parameters. Below it is shown a 3D rendering of the ISA, highlighting the main components of which it is composed. [12]

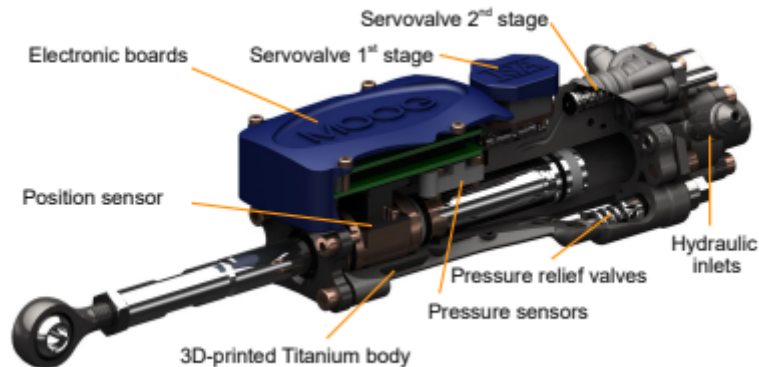


Figure 1.3: 3D rendering of the ISA, developed by Moog in collaboration with the DLS lab [1].

1.2 Stair Climbing

Stairs are in general common and difficult obstacles for robots, both in indoor and outdoor environments. In order to create a working indoor service robot, the capability to perform stair climbing locomotion is necessary. This capability includes a sufficient degree of stability and velocity, as well as robustness in the control strategy, as there exist numerous kinds of stairs, with different materials, shapes, and dimensions. Despite being more demanding than level walking, performing a stair climbing locomotion gait with a good degree of agility is key in order to achieve commercially profitable and justifiable legged robots. Stair climbing is one of the main reasons legged locomotion was profoundly studied and employed in the first place, as wheeled robot are unable to advance over steps. Numerous efforts and peculiar designs aiming at addressing this problem have been proposed in the literature; we can cite for example the curved-spoke tri-wheel mechanism employed for fast stair climbing, proposed by Kim et al. in [13], curved legs as in RHex [14], tracked as in Packbot [15], flipped track as in FlipBot [16], wheel-linkage systems as employed in the robot RHyMo [17], and so on. Each of these solutions have their own limitations, in general related to edge contact, complicated structures comprising a high number of DOFs, adaptation to different sizes of stairs, and inability to then perform a sufficiently robust and fast locomotion gait over flat surfaces [18]. The aim of this thesis work, is in part to assess this issue from a geometric and kinematic point of view, with the development of a script receiving as inputs the kinematic and geometric parameters comprising the robot, to then perform 2D simulations of the walking gaits (crawl and trot) of the robot climbing and descending the stairs, to assess the shape of the shin that allows for a highest degree of reachability of the foot. It is presented in Chapter 5, together with statistics determining the viability of the proposed design. In Chapter 4 and 7, it is presented how the results obtained through the simulations will be used to design, develop and prototype the new legs of the robot HyQReal.

1.3 Contact Sensing

In order to have real applications of legged robots, the performance of the current walking machines needs to be increased. Detractors of legged robots usually point out the platforms' speed of locomotion as among the most crucial shortcomings of these robots. A walking machine's leg needs to have the capability to work under worse load conditions when compared to a manipulator, achieve a good degree of accuracy, whilst having a weaker mechanical structure. To provide a practical example, a commercially available manipulator designed to carry a mass

1.3 Contact Sensing

of 3 kg weights approximately half a quintal, which naturally guarantees an inherently strong mechanical structure. It is although necessary to mention that there exist also lightweight manipulators, for example the UR5 from Universal Robotics [19]. In contrast, the quadruped robot SILO4's leg weighs 4 kg ca. [20], and it must be able to support up to 15 kg -half of the weight of the platform- for some particular foot positions and locomotion gaits. The floating base of these robots also poses an additional complexity in control schematics and strategies, which need to be addressed through the use of highly complex control and planning algorithms. In order to address these issues, estimation and sensing are the backbone of the design of any robotic system. From a basic level, the robot's own state has to be estimated or measured in order to introduce a feedback control strategy. To do so, multiple approaches are employed, from sensor-based readings to estimation of complex quantities based on sensor fusion and algorithms. More on that in chapter Sensors. At a higher level, perception, which is in this context defined as a task-oriented interpretation of data coming from sensors, allows the integration of information coming from a sensor across time and space with the goal to facilitate generating a planning strategy. Contact sensing technology has been under development for decades, with uses from everyday appliances, to the most advanced robotic platforms currently being developed. For the specific application of foot contact sensing applied to quadrupeds, the technology has not left laboratories around the globe until only very recently, with state of the art robotic platforms such as Boston Dynamics' Spot [21] and ETH's ANYmal C [22] making use of sensed feet to improve the capabilities, stability and locomotion in general. In chapter 3, this brief overview will be assessed in deeper detail. The second aim of this thesis, after the locomotion over stairs presented in the section above, was to assess the technologies used in the context of contact sensing applied to quadruped robots, how each of them finds uses on different platforms, how scalable they are, their pros and their cons. The analysis is aided by a linear model developed in Microsoft Excel, on which each of the parameters' significance to the final development and implementation on a production level is taken into account, and given a specific weight. By tuning some of the parameters' weights (for example response speed, cost, robot weight's effect on the durability, frequency of use of the platform, accuracy and multi-directionality of contact) it is possible to obtain a rough estimation of which of the technologies currently available are more suitable for a specific platform, making this analysis as generic (and therefore reusable) as possible.

1.4 Dynamics of Legged Locomotion

Among the most difficult tasks in the field of legged locomotion, there is the need to make the robot balance. The first questions arising are related to how to move the robot's body in order to avoid falling, with the goal to eventually reach its target location. This inherent difficulty comes from the fact that the forces of contact, defined as their location of contact and their magnitude, are necessary in order to generate control actuation strategies. They are, although, limited by mechanical laws of contact and the robot kinematics limits. By exploring the Newton's equation of motion of the robot, it becomes clear that external forces f_i are required in order to move the Center of Mass (CoM) c in a direction different from that of the gravitational acceleration g :

$$m(\ddot{c} - g) = \sum_i f_i \quad (1.1)$$

in which m is the total robot mass. Applying the Euler's equation of motion, it becomes clear that also the positions of the points of contact s_i , with respect to the CoM, are fundamental in order to keep the robot body's angular momentum L around the center of mass under control concurrently:

$$\dot{L} = \sum_i (s_i - c) \times f_i \quad (1.2)$$

In most cases contacts are unilateral, which means that the robot can only exert pushing forces on the surface of contact. Therefore, the external forces f_i can only be oriented in predefined directions, also constrained by the limits imposed by frictional action. In order to account for these constraints, it is introduced the concept of Center of Pressure (CoP) of the forces of contact, also referred as Zero Moment Point (ZMP) [23]. This point is constrained to lie in a supporting area, which is delimited by the convex hull of contact points in case the robot is standing on flat terrain, or can be computed by projection of contact wrench constraints, in more realistic and unstructured terrains [24]. Contact itself is generally considered as completely rigid, with no regard for visco-elastic deformations. This makes it so that the situation becomes binary, meaning that there is either contact or no contact. This last condition can be mathematically modeled as a *complementary condition* [25]. In case there is a collision of the leg with a surface, the load is typically impactful, and it is usually assumed in the literature that the contact point will stick afterward [26]. Although it lightens the computational load, this situation is usually undesirable. It is therefore evident the need to sense the contact, both in terms of location and magnitude [27]. In this thesis work, this challenge is approached by adding the capability to

1.5 Shin Shape Optimization

the foot to sense contact with the ground *directly*, without recurring to the use of estimation techniques, by the addition of a sensor embedded in the foot structure.

1.5 Shin Shape Optimization

Legged locomotion has been in the development for decades, and although the designs have been improved and optimized, generally the lower leg has been *left for granted*, with the most common designs being multi-piece structure, comprising of a knee, a shin, and a foot. Only recently, more complex designs appeared from around the globe, with more complex shapes and integration among the parts mentioned above. In controlled, structured environments, a straight tubular structure is the easiest to implement, it offers intrinsic strength given by the geometry, and is considered "good enough". Problems arise in real world applications though, the most compelling one being the case of stairs climbing (and, obviously, descending). In general, a straight tube affects negatively the space reachable by the robot, and if steps are not carefully planned (or in case of blindness), catastrophic failures tend to occur. Therefore, with the goal to increase the reachable space, the lower leg's shape was reimagined; not a single straight aluminum tube, but rather two segments, with relative lengths and angle as first design parameters to be optimized.

1.6 Contribution

In the context of this thesis, the problem of stair climbing and contact sensing is tackled from a theoretical and practical point of view. In order to increase the reachability of the robot, a new design of the shin is proposed based on the results coming from the script developed and described in Chapter 5. These results will be then used to aid the design of the new shin of the robot HyQReal, as presented in Chapter 7. It is also proposed a new design for the foot of the robot HyQReal, with the added capability of sensing contact with the ground through the addition of a contact sensor embedded in the foot itself, as presented in Chapter 3. The proposed design is then validated through experiments performed on the prototype, as presented in Chapter 6.

CHAPTER 2

Background

The 'Background' section provides an overview on the most recent findings in the field of legged locomotion, both in terms of design, with emphasis on the shin, and in terms of sensing technology applied to contact awareness.

2.1 Leg Design

As they are the basic components of quadruped robots, mechanical legs allow robots to excel in terms of versatility and maneuverability, to a greater extent than what is provided by the wheeled counterparts. An ever increasing amount of research is put into developing new designs, based on research coming from numerous laboratories around the globe in the last decades. In this section, some of these results will be presented, and divided in three main categories: prismatic, articulated and redundant articulated legged robots. This classification is based on the degrees of freedom the legs are comprised of.

As bionics was established as a science around the sixties, the structure, mechanism and behavior of living creatures became the objective of robotic imitation [28]. This fusion between the natural and technical world allowed to reach new frontiers in terms of adaptability and versatility of robotic platforms applied to unstructured and, sometimes, unknown environments. As such, the legged robots are robotic systems which are conceptualized as to mimic the movement and mechanical structure of the lower limbs of mammals, insects and amphibians [29]. As it is inherently a multi-limb and multi-degree of freedom structure, and thanks to its discrete motion trajectory, it is able to achieve a higher degree of stability and flexibility when compared to the most common wheeled and crawler robots [30]. In the last decade, pushed by companies such as Boston Dynamics [31], which has recently released for public sale its quadruped Spot, and it is showing the capabilities of other platforms such as Atlas with fancy and elaborate videos that can be found online. Legged robots have steadily become a hot topic in the field of robotic research. When compared to bipeds, quadruped robots achieve a higher level of stability and load capacity, and has a larger leg movement space, while requiring less mechanical redundancy and in general a lower degree of complexity when compared to multi-legged (more than 4 legs) robots [32]. Some of the parameters of relevance of some of the most famous quadruped robots developed in recent years is reported in Table 2.1. By analysing the data reported in the table, it is noticeable that the current robots are still far from perfect, as they still lack a sufficiently high locomotion velocity, and a low payload-to-weight ratio. All data reported is publicly available online.

As it is a fundamental part of quadruped robots, the mechanical legs determine some of the core performance indices for the overall platform, of which we can cite locomotion velocity, load capacity and terrain adaptability [33]. Therefore the current designs still need to be improved, as they currently lack the expectations provided by the animal counterparts. Some of the most critical indices in this sense, that need to be improved in the future and present, as they are still far from satisfactory, include power density, mechanical strength and energy efficiency [34].

2.1 Leg Design

Robot	Weight (kg)	Payload/weight	Max. speed (km/h)	Year
BigDog	109	0.41	10	2008
HyQ	90.4	—	7.2	2010
LS3	590	0.3	11.2	2011
WildCat	154	—	32	2013
TITAN-XIII	5.2	0.2	3.6	2013
Cheetah-cup	1.1	—	5.1	2013
Spot	75	0.6	—	2015
SpotMini	30	0.47	—	2016

Table 2.1: The weight, payload-to-weight ratio, and maximum speed of significant quadruped robots in recent years [10].

2.1.1 Prismatic Leg

The design methodology of prismatic legs is one of the "oldest" in the field of modern robotics. Successfully applied designs date back to the eighties, when they achieved and kept the record of locomotion velocity for quadruped robots at that time [35]. In this case, the leg mimics the bouncing of an animal's leg by a simple, single rod configuration. In terms of topology, the structure is composed of a rotative joint, hinged at the hip joint, and a prismatic joint. The prismatic joint can be applied by means of a hydraulically actuated piston in line with an air spring. The pros of the hydraulically actuated piston are, to cite a few, the low response time, the high degree of precision control, the great level of precision adjustment, and the high output force (which is inherently higher, at comparable volumes, than the electric counterpart). The benefits of including the air spring include the ability to absorb impact loads, and bottom impact energy reduction by means of an air cushion. Another way to implement the prismatic joint is through the use of a motor-ball screw-spring mechanism, as developed Ahmadi and Buehler in [36]. The periodic drive of the linear motor allowed to reach a compliant drive, allowing for a quasi-static vertical oscillation of the leg. In other designs, the prismatic joint was a simple passive spring, as that developed by Poulakakis et al. in [37]. As the mechanism does not require a drive, it is more compact and lightweight compared to the alternatives presented above, while also being more robust in case of multiple impact loads and compliant operation. The topology of the structure is reported in Figure 2.1. [38]

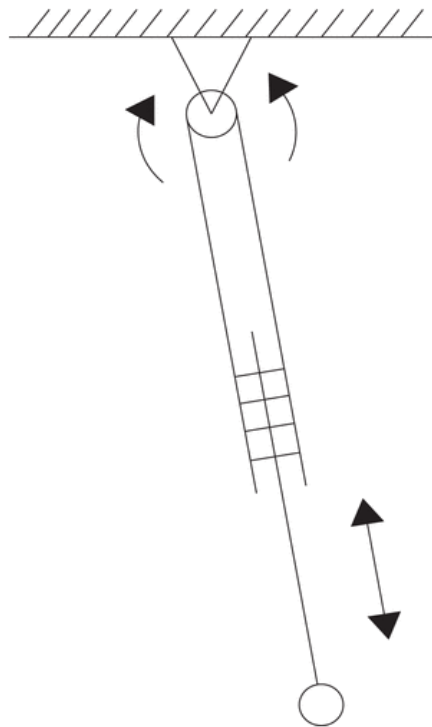


Figure 2.1: Prismatic Leg topology [2]

2.1.2 Articulated Leg

Differently from the prismatic leg, in order to achieve the telescoping movement, the articulated leg make use of a rotating joint in place of the prismatic one, in order to achieve control over the length of the leg. The functionality is very similar to that of the knee and elbow found in animals, and it provides good biomimetic characteristics. The main subdivision found to describe the kinds of articulated legs, is between the mammal and sprawling type, based on the configuration of the leg [39]. The sprawling-type leg is characterized by the upper limb (the thigh) being oriented horizontally, while the lower limb (the shin), is vertical in the nominal pose. In contrast, the mammal type means that both the limbs are placed vertical to the locomotion plane as the nominal pose. Figure 2.2 depicts the differences between the two types in terms of geometry and kinematics of the limbs. In general, mammal-type legged robots are able to achieve a higher locomotion velocity, a lower driving torque and a smaller footprint. Sprawler-type, on the other hand, are able to achieve a better stability, improved safety and a wider range of motion.

Boston Dynamics proves once again pioneer in developing successful legged robots employing articulated legs, with platforms such as Spot, Spot Mini, LS3, BigDog and WildCat. The exact specifications of these robots are not made public, and can only be assumed from the footage

2.1 Leg Design

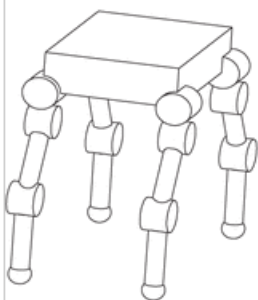
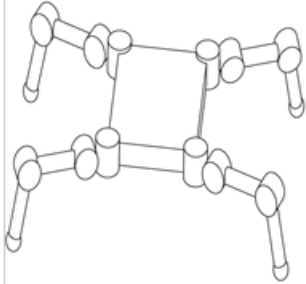
Topology	Characteristics
	(a) Mammal-type robot (b) The joint torque is small when the leg is bent, and there is almost no joint torque when standing upright. The footprint is small, and it is easy to pass through narrow spaces
	(a) Sprawling-type robot (b) The front and rear swings are large. The center of gravity can be adjusted to a low position. The body can be used as a support point while standing

Figure 2.2: Articulated legs types [3]

released by the company and found online. WildCat and LS3 makes use of an internal combustion engine to generate the propulsion, the Spot series employs electrical motors. The two-stroke gasoline engine of these two platforms is able to achieve a very high power density, but are subject to high fluctuations of speed and torque due to the nature of the engine. In order to compensate for this, these robots are equipped with hydraulic accumulators to serve as energy reservoirs, and like this they are able to provide immediate response power and a reduction in oil pressure fluctuations. A disadvantage of using an internal combustion engine is the high level of noise and vibration, which hinders the capabilities to employ on field these platforms, especially for military applications which, we recall, are among the driving forces behind the success of the aforementioned company. The Spot series, in contrast, employs electrical motors powered by batteries. In order to reduce the overall inertia of the leg assembly, the knee motor can be placed at the hip level, and through a traction mechanism the power can be then transmitted to the distal joint. The hydraulically driven quadruped robot HyQ, the grandfather of the robot this thesis aims at improving, uses electro-hydraulic articulated legs. The configuration is shown in Figure 2.3.

The benefits of this hybrid configuration are the combination of high speed and torque provided by the hydraulic system, and the compactness of the electric actuator. This configuration is also able to achieve a great degree of reliability when experiencing torque peaks, which are

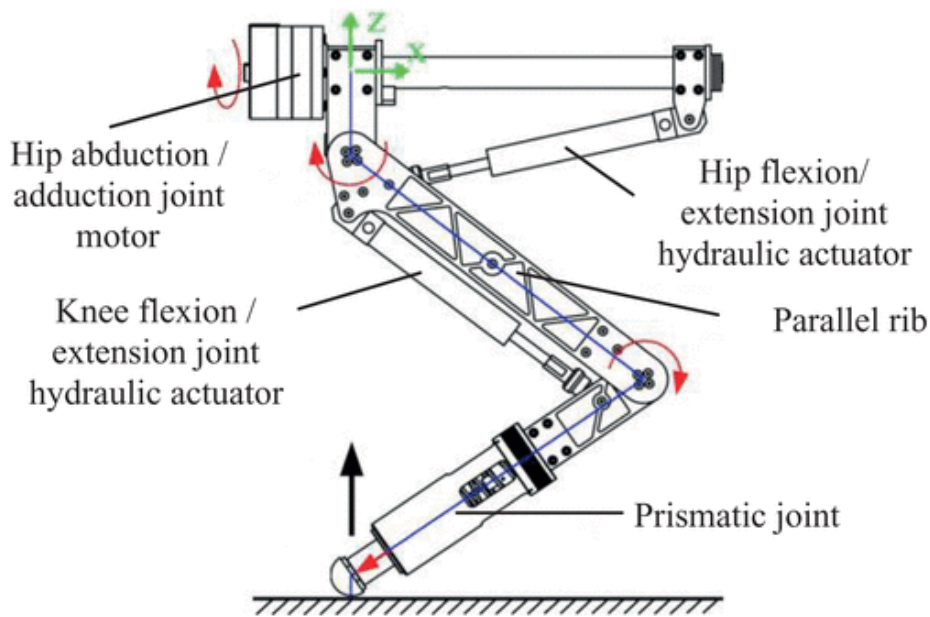


Figure 2.3: HyQ articulated leg [4]

required for the hip flexion and extension joint (HFE) and the knee joint (KFE), as well as allowing for a good compactness of the hip abduction/adduction joint structure (HAA). The HAA joint is comprised of a tubular structure and a multitude of bearings, which aid in distributing uniformly the loads and to achieve a backlash-less connection between the body and the leg of the robot. The HAA structure was later improved in the robot HyQ2Max, as it was achieved a wider range of motion, together with improved locomotion velocity, higher resistance to impact loads, and better payload carrying capability.

The HAA joint makes use of a double vane rotary hydraulic actuator, and it allows dual torque characteristics, at the price of a reduced range of motion. The HFE joint comprises a single vane rotary actuator, which allows a higher range of motion but reduced torque output. In order to drive the KFE, a linear hydraulic actuator in conjunction with a four bar linkage was developed. It should be noticed that the four bar linkage proves to be a good match to the hydraulic actuator, because it can handle effectively the high loads and torques during the extension of the leg, and the low torques that occur during the retraction phase.

One last example is the ANYmal quadruped [22], which employs highly integrated series elastic actuators (SEA) to drive the legs. These actuators fuse a high-torque motor, a gearbox and a rotational spring together with sensors, electronics and bearings. Therefore, the mechanical structure is compact and robust, not requiring any additional mechanical components. Among the benefits of employing such technologies is that they allow for a complete rotation of the joint around its axis of rotation, thus improving the versatility and mobility of the platform.

2.1 Leg Design

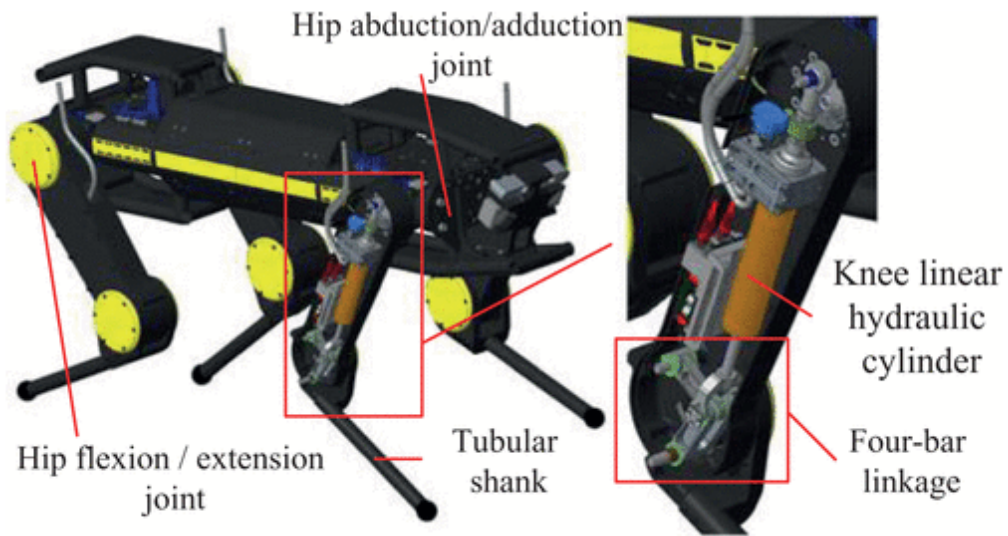


Figure 2.4: HyQ2Max [5]

2.1.3 Redundant Articulated Leg

The redundant articulated leg's configuration is comparable to that of the articulated leg, with at least an additional rotary joint applied to the joint before the end effector. This configuration can be found in nature, for example in toed or hooved animals, and it achieves a higher degree of biomimicry and kinematic properties for this reason. In literature, the most common redundant articulated leg comprises three rotary joints [40], but other configurations are also possible, by making use of prismatic and mixed joints [41]. The mechanical leg comprises thigh, shank, and foot, connected by hip, knee, and ankle joints. Proper design of each link structure can allow the robot to achieve a large payload-to-weight ratio, while providing good resistance to impact loads. The toe has a rubber pad that provides shock absorption when in contact with the ground, while also increasing the frictional properties between the ground and the foot, thus improving horizontal propulsion. The actuator consists of a brushless DC motor, a ball screw, and a die-compression spring, allowing backdrivability and the ability to withstand shock and vibration, while providing a good force control at the joint. These characteristics are largely beneficial to the adaptability to the ground in high-speed motion. In order to achieve a more natural movement and improve leg-to-ground interaction, to provide an example, a magneto-rheological (MR) rotary brake is integrated at the knee joint. The MR brake consists of an outer housing, the MR fluid and a rotor jointed to the knee joint axis, and utilizing the rheological property of the fluid to produce different rotor braking torques can provide controlled viscous rotational damping [42].

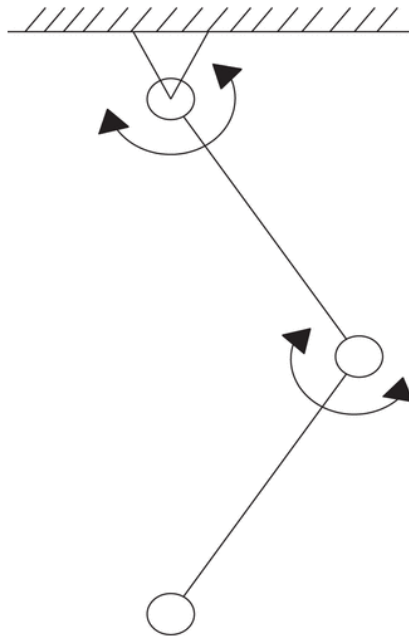


Figure 2.5: Articulated Leg topology [2]

Through the example analyses presented above, it is possible to derive the following conclusions. The prismatic leg type simplifies the control algorithm, and there is much diversity in choosing the telescopic actuators. Examples of which are pneumatic actuators, hydraulic actuators, and motor screws. The leg structure is the simplest and lightest, providing the lowest inertia. However, this leg configuration limits its own kinematic performance, as it comprises fewer rotating joints, resulting in insufficient adaptability to different kinds of terrain. The redundant articulated leg is similar to the toed or hooved animal legs observed in nature. It achieves better bionics in geometric topology, better motion performance, greater self-stabilization speed domain, wider leg-foot motion space, and higher energy efficiency. It shows greater advantages in complex terrain adaptation and obstacle crossing. However, introducing more rotating joints comes at the cost of additional actuators, not only increasing the complexity of the controller structure, but also placing higher demands on sensing and leg structure design. Reducing the inertia of the distal leg is a problem that must be considered. The articulated legs are located between the prismatic legs and the redundant articulated legs in terms of motion performance, structural complexity, and ease of control and have the best balance between complexity and performance, thereby this type of leg is currently used more on quadruped robots [2].

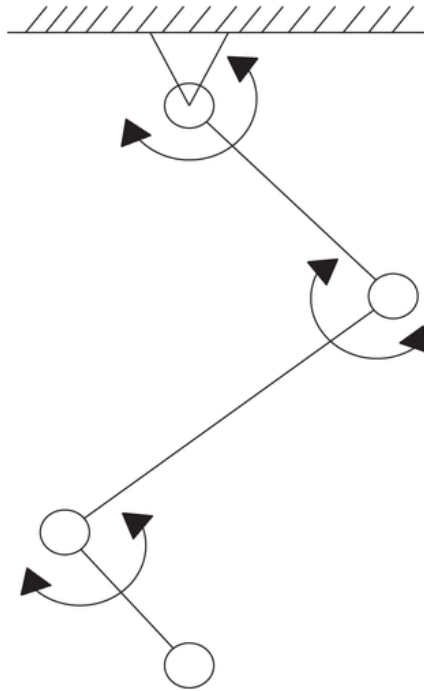


Figure 2.6: Redundant Articulated Leg Topology [2]

2.2 Contact Sensing Technologies

In Chapter 3 will be presented the trends in research on the field of contact and force sensing technologies, in this context applied to ground reaction forces estimation. Sensing contact with the ground is fundamental in order to ensure stable contacts and stability of the robot [43]. The terrain characteristics and area make compliance a necessary feature in order to protect the robot against unexpected disturbances from either human or environment factors. Although position control can produce accurate motion, it relies on a perfect knowledge of the environment in which the robot is navigating, in order to provide a planning of the swing leg trajectories, which is impossible to obtain. In case the robot is walking on an uneven terrain or slope, the swing leg may strike on an obstacle or land earlier than planned. This impact creates additional perturbations to the whole kinematic chain and might cause the robot to lose balance or stability [44]. In this context, active contact sensing becomes an impelling problem to be addressed, and to be solved. One of the goals of this thesis is to use this as a starting point to add the capability to sense contact with the ground to the robot HyQReal, and the results of this analysis, together with the proposed technology aiming at solving this problem, are presented in the next chapter.

CHAPTER 3

Sensors

The focus of Chapter 3 is to provide an overview on the contact sensing methodologies used as state of the art in the research and industrial field of robotics. At first, it is provided an overview on the concepts of perception and estimation, to then focus the attention of the reader to the more specific case of contact sensing applied to the detection of ground contact of legged robots. It is finally proposed a model aiming at aiding in the choice of the most appropriate sensor for this task, and how this was applied for the robot HyQReal.

3.1 Introduction

In order to accomplish successful real applications of walking robots, the performance of current walking machines needs to be improved.

Controlling a robot would be relatively easy, if a complete model of the world (defined as the environment in which the robot's action is executed) was accessible, and if the robot's actuators were able to execute commands in a perfect manner. Unfortunately, a complete model of the world is usually not available, and perfect control of mechanical structures is *never* a realistic assumption. In order to compensate for this absence of complete information, the most common and successful approach makes use of estimation and sensing. The role of the latter two is to provide information regarding the state of the robot, as well as that of the environment, in order to form the fundamentals for controlling strategies, decision making, and interaction with external agents, such as humans. It should be noted that there is a substantial difference between when estimation and sensing is used to recover the state of the robot itself, which is defined as *proprioception*, and when these tools are used to recover information about the external world. In the latter case, we talk about *exteroception*. Generally, the majority of robotic systems are designed to have a degree of proprioception high enough to estimate and control their own physical state; but on the other hand, being able to recover and use in real time the state of the environment based only on sensor data is generally a much more complex problem to handle. Some of the earliest works on the field of computational perception applied to robotics assumed that one would be able to recover a complete and generalized model of the environment, to use such a model to guide the decision making process, and then act on it, as for example discussed in the book "Vision", by D.C. Marr [45].

It has become apparent, in more recent developments in the research field, that using such an approach to solve these problems is highly unrealistic. In fact, keeping in mind that sensor-based robots now appear in the most diverse fields of application (from medical to surveillance to manipulation), it has become clear that appropriate use of sensing technologies and estimation for a given system must be highly task dependent [6]. When speaking of estimation and sensing in the same context, it is speaking of the process of transforming a physical (measurable) quantity into a computer representation, which will be then used at other levels for further refinition. Sensors are inherently closely bonded to transducers, which are components used to translate a physical quantity into a signal that can be processed by a computer. Sensors are also inherently closely related to perception, which is the way in which sensory information is represented in a task-oriented model of the environment. Although the approach is extremely promising and open to uncountable applications, it *must* be kept in mind that data coming from sensors in usually

3.1 Introduction

affected by numerous external and internal factors that modify the reading, making the process non trivial. To name a few, discretization is introduced in the process of digitalization, statistical noise is inherent in transducers, and ambiguity coming from poor sensor selectivity might also be introduced. To mitigate this uncertainty, estimation methods are therefore established to aid in the process of proper integration of information into models that simulate the world, and to improve the SNR (Signal to Noise Ratio). In the following sections will be presented the rationale followed in choosing the appropriate sensor in order to add the capability to sense contact with the ground to the robot HyQReal. The dissertation will start with an overview on the state of the art progress on the concept of perception and estimation, to be then followed by an overview on the commercially available sensor solutions, from the simplest to the most advanced, their pros and their cons, and the rationale that was followed in order to make an educated guess on the choice for the robot HyQReal [6].

3.1.1 Perception

When talking about the input to the perception process, there are generally two things happening at the same time: both digital data coming from multiple sensors/transducers, and a partial model of the world containing relevant information about the robot's structure (geometric, kinematic, and dynamic) and state related to the world taken under consideration. In Figure 3.1 (courtesy of the Handbook of Robotics, edited by Springer), the perception process is structured as to include the most common operations which are applied in order to integrate data coming from sensors and the environment model. As it is a general view, some of the blocks might obviously differ, based on the task taken under consideration, or be missing altogether. However, the model shown should be enough to depict the most of the problems arising from estimation and sensing. The first issue encountered is related to feature extraction, and preprocessing, which is a process by which noise coming from the sensors and transducers is reduced (or eliminated altogether, when possible), and to highlight key characteristics of the signal acquired. The next step in the process is to match (associate) the data with a predefined model which might be based on a structure known in advance (for instance a CAD model of the world, or a recreation built upon data acquired a priori from other sensors). Matching methods are generally used in order to evaluate the kind of relationship that exists between data coming from sensors, and the world model.

Once this data has been associated to the environment model, it is then attainable to update the model with the most recent details coming from the sensors. For instance, the pose of an end effector can be updated in the simulated world with the latest reading coming from the encoders located in the joints of the manipulator.

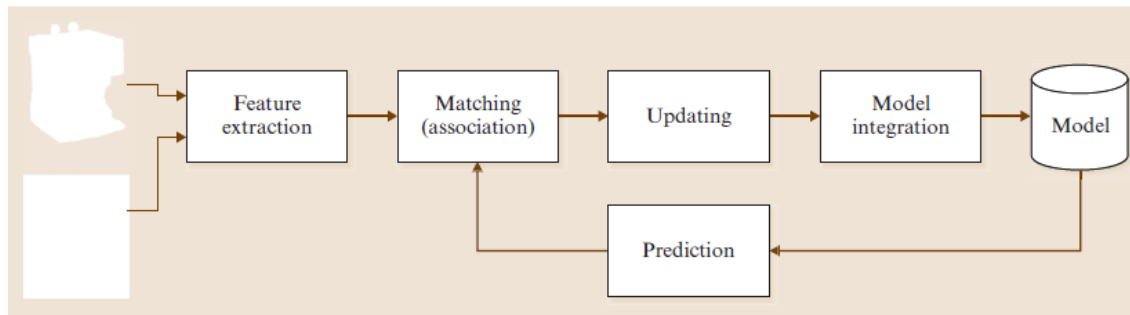


Figure 3.1: Perception Loop [6].

At last, it is achievable to expand the model to a dynamical system one, highlighting the fundamental states being estimated. Using such a system-centered model, it is then possible to make a prediction on how the environment evolves over time, until a new cycle is initiated with new data from sensors.

3.1.2 Estimation

Robotics inherently deals with things that move around in the environment. We live in a time of rovers furrowing Mars ground, self-driving cars and drones surveying the Earth. The field of robot ethics is trying to answer legitimate questions on how this technology is used and the social and psychological implication of using such technologies for unethical and totalitarianistic antidemocratic uses. Although specific robots have their own strengths and weaknesses, it is common to face issues when dealing with manners such as *state estimation* and *control*. The state of a robot is defined as the set of quantities that, when known with accuracy, allow to describe in a complete manner the robot's motion over time [46] [47]. At the current state of research, the majority of the work done in the field of state estimation applied to legged robots is based on filters fusing together a multitude of sensor modalities, such as leg odometry, which employs kinematic measurements and high frequency inertial measurements, together with lower frequency modalities used to assess and correct the drift (for example using LIDAR or cameras). As previously discussed, there exist numerous techniques by which information coming from sensors can be combined. How this techniques are used and combined depends, by a great extent, on what is previously known about the world, what informations are necessary to perform the required task, and what are the most appropriate models for the sensing system in use. Commonly used methods make use of simple voting-based methods, parametric and nonparametric statistical estimation methods, and fuzzy-logic systems [48]. At the current state of research, the majority of the work done on state estimation applied to legged robotics is designed such that it assumes a rigid contact with the ground, while not accounting for the physical charac-

3.2 Choice of Sensor

teristics inherent in different kinds of terrain. Some of these characteristics include, but are not limited to, terrain impedance and coefficient of friction. Achieving a reliable state estimation is proving to be key in order to advance the state of research, and to finally deploy platforms that are affordable and reliable. Furthermore, a good degree of state estimation is key not only in the field of locomotion (in this case we talk about low-level state estimation), but also for task dependent applications, such as exploration and navigation (in this case we will refer to task-level state estimation) [49].

3.2 Choice of Sensor

There are many ways in which sensors can be catalogued, depending on what they measure, and in which way this measurement is performed. As mentioned in the previous section, in general it is possible to divide sensing technologies in proprioceptive and exteroceptive. Proprioceptive sensors are those that are used to measure the internal state of a robot, might that be a value of temperature, force applied to an end-effector, position of various degrees of freedom, and so on. Exteroceptive sensors, on the other hand, are those that are used to gather information regarding the external world in terms of distance, force interactions, external pressure, and so on. Another way to differentiate sensors, is to define whether they are active or passive: an active sensor is one that is able to release energy to the environment, and to measure the properties based on how the world responds to these excoming signals. Passive sensors are, on the contrary, those that are not active. This means that, in order to measure a certain quantity, they must rely on something they cannot exert a control upon. This makes, in general, passive sensors less robust and reliable compared to active ones [50]. That being said, it is not like active sensors are immune to disturbances when evaluating a certain quantity: to give an example, a structured light system is able to project a pattern upon the scenery and is therefore less prone to errors due to the characteristics of the scenery analyzed; but are still sensitive to scattering, absorption and interference of the signal they emit, and this can negatively affect the performance of the sensing unit. When talking about proprioceptive sensors, it is common to find out that passive-type are used. Among the uses, the most relevant physical properties of the robot that are measured are generally related to torque, position, velocity and acceleration, to name a few. In chapter 2, it is discussed how torque sensors are used to estimate contact with the ground for the robot HyQ (and then HyQReal) at the DLS lab, at IIT in Genova, where the work presented in this thesis took place. On the other side there are exteroceptive sensors. These can be further divided in contact-based and non-contact type. Contact-based sensors are, in general, employed in the same ways as proprioceptive sensors, while non-contact ones make use of many ways to measure

a physical quantity at a distance. The kind of properties that can be measured without the need to have a physical contact are, to name a few, range, direction, intensity and size.

3.2.1 Snap-Action Switches

The first contact sensor considered was also the cheapest and simplest: the bump switch, also known as snap-action switch. In general, this single-pole, double-throw (SPDT) momentary switch can be used as a general-purpose micro switch or tactile bump sensor for robotic applications. Despite the benefit of a very low cost, ease of installation and simple communication (ON/OFF signal only), this option was eventually discarded due to being prone to rupture in case of overloading, a common occurrence during locomotion of the robot HyQReal, with impact loads above 1000 N in the worst conditions [51].

3.2.2 Load Cell

Load cells, in conjunction with a strain rosette, are a common way to measure loads on components, by measuring the deformation of the material on which strain gauges are fixed. Among the benefits of the strain gauges configuration, we can cite the accuracy in reading along the X and Y direction (the plane on which the strain gauge is fixed), and the high degree of responsiveness to applied load. These benefits are however overshadowed by the high cost of installation, as they require custom shaped supports in order to provide a reliable reading, usually in hardly reachable locations in order to exploit the points of higher strain, the high weight due to the supports just mentioned, the difficulty to read reliably along the normal direction (Z axis), and the fact that they are inherently prone to false positives, as they are affected by inertial effects.

3.2.3 Force Sensitive Resistors

A Force Sensing Resistor, also referred by the initialism FSR, is a kind of material whose electrical resistivity changes when a force, a pressure, or a mechanical stress is applied to its surface. Normally, a FSR is provided as a polymer sheet or ink that can be applied by screen printing. The sensing film comprises both electrically conducting and non-conducting particles suspended in matrix. The particles are sub-micrometre sizes, and are formulated to reduce the temperature dependence, improve mechanical properties and increase surface durability. Applying a force to the surface of the sensing film causes particles to touch the conducting electrodes, changing the resistance of the film. As with all resistive based sensors, force-sensing resistors require a relatively simple interface and can operate satisfactorily in moderately hostile environments. When comparing FSRs to other commonly employed force sensors, the advantages of this technology

3.2 Choice of Sensor

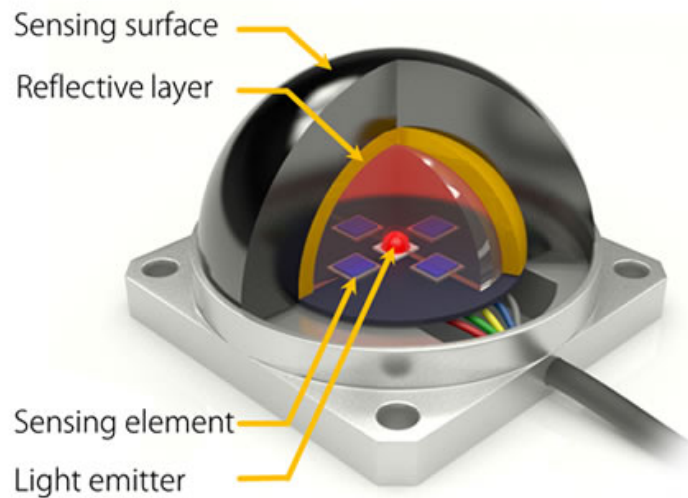


Figure 3.2: OptoForce sensor, image courtesy of OptoForce Ltd.

use are related to their size, with thickness generally less than 0.5 mm, low cost and good shock resistance. A disadvantage is their low precision: measurement results may differ 10% and more. Furthermore, force-sensing capacitors offer superior sensitivity and long term stability, however they require more complicated drive electronics and they are prone to experience sensitivity degradation. FSRs were considered good candidates for the contact sensing implementation, but they were eventually discarded due to their low force threshold being, for custom-made ones, about 150 N before rupture [52].

3.2.4 OptoForce

In optical force sensors, photodiodes are used in order to measure the quantity of light, originally emitted by an LED located at the center of the hemisphere, reflected on the reflective layer. The forces can then be precisely reconstructed by measuring the values on each of the photodiodes. One great advantage of using this technology is the fact that the resultant force is not only given in magnitude, but also direction. One other great advantage of optical force sensors is the fact that, in general, they are more robust than their counterparts, for example load cells, while being lower in weight. This is achieved because the deforming surface is physically separated from the sensing element, as infrared light is used in order to detect the deformation in the shape of the sensing surface [53]. This solution, although the most promising in terms of reliability, isotropic in reading force from multiple directions, and robust, was eventually discarded due to its high cost.

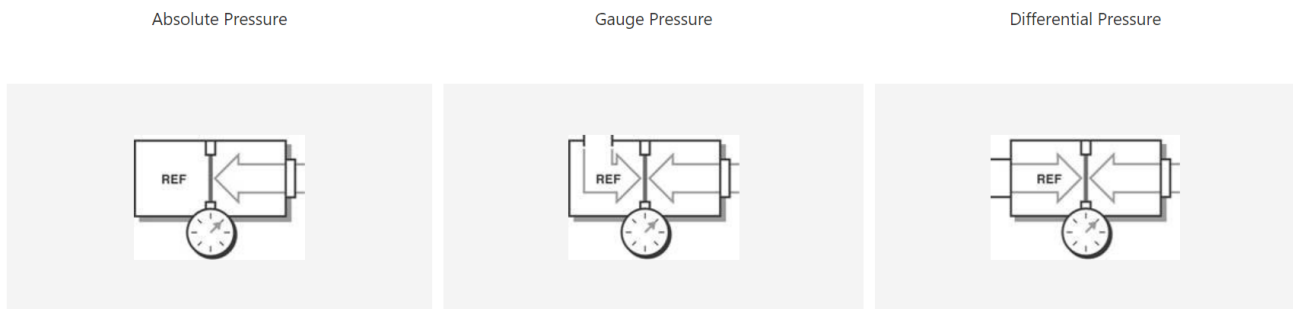


Figure 3.3: Pressure measurement techniques, comprising absolute, gauge and differential measuring methodologies [7]

3.2.5 Pressure Sensors

Pressure is defined as force per unit area that a fluid, a solid, or a gas, exerts on its surroundings. Pressure, is a function of force, and area:

$$P = F/A \quad (3.1)$$

Where P stands for Pressure, F stands for Force, and A stands for Area. In the International system of Units (SI), pressure is measured in PascalS N/m^2 , but alternative units of pressure are commonly used. These include, but are not limited to, pounds per square inch (psi), atmospheres (atm), bars, millimeters of mercury (mm Hg), inches of mercury (in. Hg), and torr.

Pressure can be measured either statically or dynamically. When there is no motion involved, it is referred to static pressure. Static pressure can be found in for example when measuring the pressure of air inside an inflated balloon, or water inside a tub. Often, a fluid in motion affects the magnitude of the force applied to its surroundings. To give an example, the pressure of water inside a hose with the nozzle closed is about 2.6 bars. Opening the nozzle has the effect of dropping the pressure to a lower value as water is poured out. In order to properly and effectively measure pressure, the circumstances under which the measurement is made must be accounted for. Among the factors are included flow, fluid compressibility, and external forces. These factors can all affect pressure in some ways.

Absolute Pressure

When measuring absolute pressure, it is referred to as measuring relative to 0 Pa, the static pressure in a vacuum. The pressure that is being measured is acted upon by atmospheric pressure in addition to the pressure to be measured. Therefore, absolute pressure measurement includes the combined effects of atmospheric pressure. This kind of measurement technique is suited for

3.2 Choice of Sensor

the application of atmospheric pressures detection, with uses in altimeters or vacuum pressures. Often, to describe absolute pressure it is used the abbreviation Paa (Pascal's absolute).

Gauge Pressure

Gauge pressure, differently from absolute pressure, is measured relative to ambient atmospheric pressure. This implies that atmospheric pressure acts upon both the reference and the pressure to be measured. For this reason, gauge pressure measurement excludes the effects of atmospheric pressure. Applications of this measurement technique include tire pressure and blood pressure measurements. Similar to absolute pressure, to describe gauge pressure it is used the abbreviations Pag (Pascal's gauge).

Differential Pressure

Differential pressure is in many ways alike to gauge pressure; however, the reference is another pressure point in the system instead of the ambient atmospheric pressure. This method can be used in order to keep relative pressure between two containers such as a tank and an associated feed line. Also, as in the cases reported previously, to describe differential pressure the abbreviations Pad (Pascal's differential) is used. Differences in conditions of measurement, materials employed in the construction of a sensor and ranges lead to a wide variety of designs of pressure sensors. It is possible to convert a pressure reading to some intermediate form, for example displacement. This can be measured by measuring the deflection of a diaphragm located in line with the fluid. This displacement is then converted into an electrical signal, which can be voltage or current. Knowing the area of the diaphragm, pressure can be then calculated using the canonical equation relating force and area. Pressure sensors comprise a scale providing a method useful to convert to engineering units. The three most universal types of pressure transducers are the bridge (strain gauge based), variable capacitance, and piezoelectric.

Bridge-Based

Wheatstone bridge, or strain based sensors, are the most common pressure sensors in the market, as they offer solutions on a wide spectrum of accuracy, size, ruggedness indicators, and cost constraints. Bridge-based sensors are able to measure absolute, gauge, or differential pressure in a wide range of pressure sensing applications. A strain gauge is used in order to detect the deformation of a diaphragm, which is subjected to the applied pressure to be measured.

Capacitive Pressure Sensors

Variable capacitance pressure transducers measure changes in the capacitance between a metal diaphragm and a fixed metal plate. The capacitance between two parts changes if the distance between these two plates varies due to the pressure applied.

Piezoelectric Pressure Sensors

Piezoelectric sensors exploit the electrical properties of quartz crystals instead of resistive

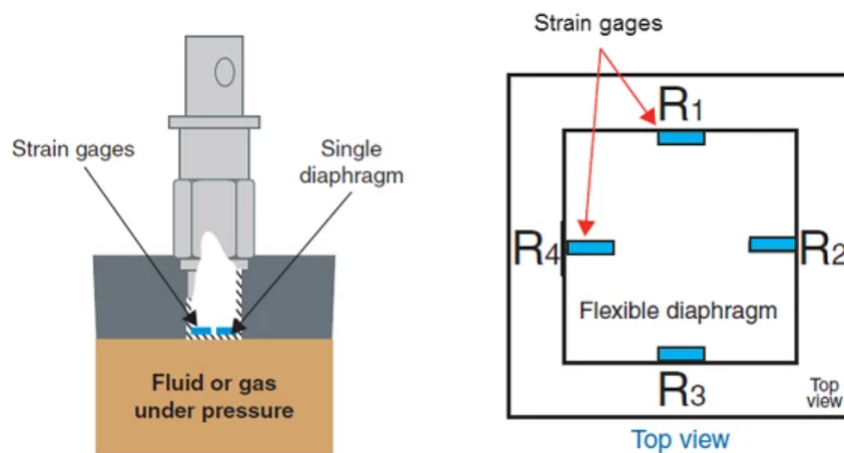


Figure 3.4: Bridge-based pressure sensor [8].

bridge transducers. These crystals are able to generate an electrical charge as they deform due to a stress (strain). Electrodes are then employed to transfer the charge from the crystals to an amplifier built into the sensor. An external excitation source is not required when using this sensor technology, but they tend to be susceptible to shock and vibration.

3.2.6 Pressure Measurement Methods

A pressure measurement can be described by taking into account the measurement types that are being performed. The three most common methods used in order to measure pressure are absolute, gauge, and differential. Absolute pressure is referred to the pressure in a vacuum, while differential and gauge pressures are computed respect to another pressure, that can be the ambient pressure or pressure in an adjacent pressurized tank.

In order to obtain proper manipulation and grasping capabilities, tactile sensing is widely considered as a crucial capability. Parameters such as contact pressure distribution, as well as the location of object contacts, are often considered as fundamental to ensure effective manipulation, and locomotion, over unstructured environments. Despite the technology's promising applications, and the availability of commercial solutions available on the market, the experimental progress has been limited in using tactile information to provide contact sensing, and to control grasping manipulation. Many reasons can be given to explain this situation, but for sure one of the most crucial factors is the high cost and complexity of integrating tactile sensing into robot feet (and hands). Dozens of publications are available in the robotic literature, but in order to implement such sensors in the final product, custom solutions are required, and the fabrication usually requires nonstandard manufacturing processes. Some of the newest, and most

3.3 Sensor choice for HyQReal

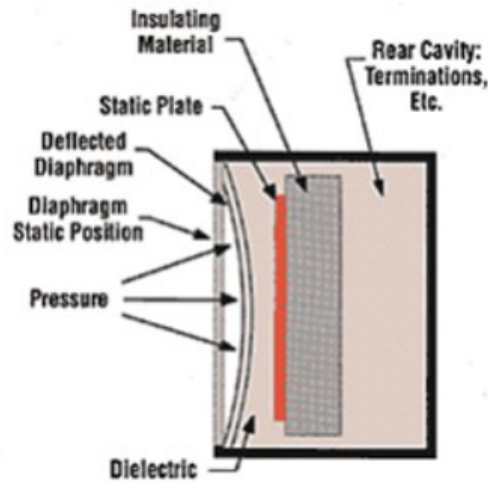


Figure 3.5: Capacitive pressure sensor [7].

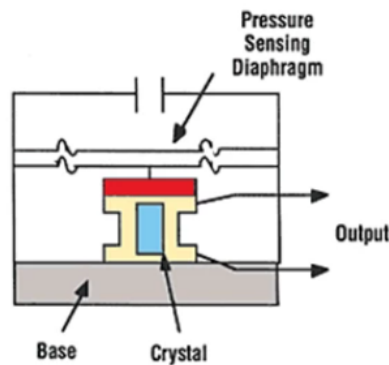


Figure 3.6: Piezoelectric pressure sensor [9].

promising, ways to implement such technologies make use of pressure sensors embedded in the end effector. Pressure sensors are cheap, robust, and provide linear outputs over their range.

3.3 Sensor choice for HyQReal

In the previous section were depicted the contact and force sensors explored before making a final decision on which way to pursue, to add the capability to sense contact with the ground to the robot HyQReal. In order to make an educated guess on which would be the most effective solution, a model was developed to aid in the decision process. Parameters were chosen, and a weight was assigned to each of them. The first table shown in the following page provides the results of the analysis, while the second explains the choice of weight for each of the parameters.

Force/ contact sensors relevant parameters				
Parameters weight	4	3	2	1
Response time	0-10 ms	10-50 ms	50-100 ms	≥ 100 ms
Durability	shock resistance, fatigue resistance	shock resistance	need precaution	fragile
Accuracy	Full range, High sensitivity (± 1 N)	Full range, Limited sensitivity (± 10 N)	ON/OFF, Trigger ≤ 10 N	ON/OFF, Trigger ≥ 10 N
Price	≤ 10 €	10-100 €	100-500 €	≥ 500 €
Weight	0.1-10 g	10-100 g	0.1-0.5 kg	≥ 0.5 kg
Time to implement	stock	stock+stock	stock+novel	novel
Contact	NO	/	YES	/
Inertia influence	NO	/	YES	/

Table 3.1: Force/Contact sensors parameters of relevance considered in the analysis

	response time	durability	accuracy	price	weight	time to implement	contact	inertia	TOT
Basic Switch	4	3	2	4	4	3	3	2	25
MRE	4	2	4	2	3	1	3	4	23
Inductive Proximity Sensor	4	4	3	3	2	2	4	2	24
Load Cell	4	2	3	2	2	3	3	4	23
FSR	4	1	3	4	4	1	3	4	24
Optical Sensor	4	4	2	2	3	2	4	4	25
Pressure Sensor	2	4	3	4	4	2	4	4	27

Table 3.2: Results of the analysis aimed at choosing the most appropriate force/contact sensor. The highest the total score, the better.

CHAPTER 4

Mechanical Design

Chapter 4 is devoted to presenting the mechanical design of the new foot and shin of the robot HyQReal, with focus on materials chosen for the new foot, and numerical analyses performed to assess the performance of the design.

4.1 Preamble

Before starting with technicisms, let us spend a few words on the natural world, since, to quote Khalil Gibran, "Forget not that the earth delights to feel your bare feet and the winds long to play with your hair". Understanding how animals evolved and adapted to survive -thank you Charles Darwin- is of fundamental importance in order to have a direction to guide us in designing something new, and to strive for perfection. The robotic platform that this thesis aims to improve is one of the heaviest quadruped robots being developed worldwide (well over 100 kg compared to the 31.7 kg mass of the commercially available Spot from Boston Dynamics). This is mainly due to the fact that, being hydraulically actuated, it comprises a couple of hydraulic units (HPUs) and a battery pack to drive them, as well as the electronics and the mechanical structure to support and protect it all. The robot showed its potential in the publicly available video [54], in which it has demonstrated its capability to generate enough force to pull a small passenger airplane (Piaggio P180 Avanti), with a mass of 3300kg.

4.2 Foot Design

4.2.1 Choice of Materials

In designing the new foot for the quadruped robot HyQReal, there were some constraints mainly related to the shape, as it was requested to maintain a spherical shape, which is a standard in quadruped locomotion. The spherical foot is widely used mainly because it ensures an easy and convenient control strategy for the leg. However, the foot size should not be too small, otherwise it will cause excessive subsidence in contact with soft terrain [55]. One other constraint to the design was that the new version of the foot would have an inherent stiffness close to that of the base design. To evaluate the theoretical stiffness of the foot, simulations were run on Ansys Mechanical software to evaluate the deformation and the reaction forces in case of contact with the ground. The model used was a simplified version of that currently used on the robot HyQReal, to lighten the computational complexity of running such simulations.

4.2.2 3D CAD Design

Once the sensor was chosen, as presented in the final section of chapter 3, the following step in the process was to make a 3D model with the characteristics required by the sensor in order to obtain a suitable reading at the desired threshold. To recall (see chapter 3 for more insights), the final choice was to use a pressure sensor, which would provide a reading through a minimal

4.2 Foot Design

deformation of a control volume (air in the first prototype) embedded in the foot itself. The design goals were to have a stiffness comparable to that provided by the current foot, a volume deformation of the control volume high enough to provide a sensible sensor read, and the 3D models used for prototyping were created using the software for Computer Aided Design (CAD) NX from Siemens. To validate the viability of the proposed designs, the models were then exported, to be then tested through numerical simulations using the software Ansys. Below are reported some of the tentative designs, their criticalities, and how failures guided the design process to reach a satisfactory result, which was then produced and used for the experiments (more on that in Chapter 6).

Baseline

As a starting point, it is reported a section view of the current iteration of the foot:

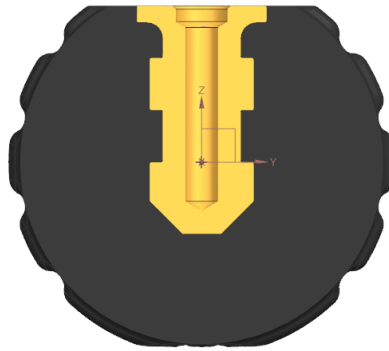


Figure 4.1: Cross section of the foot, as currently used in the robot HyQReal

It comprises a two-pieces structure, with the external volume made of rubber (with shore hardness varying from 30A to 90A, depending on the version), and an internal brass pin which also acts as contact interface with the rest of the leg. The foot is produced through the use of vacuum molding technique.

First Design: Sphere

Sphere was the name given to the first control volume chamber design. The design was trivial, as it comprised a simple sphere located 5 mm below the center of the toe. In this phase of development, the pin was left unchanged, but that would have changed in the subsequent stages of design. The criticalities of this proposed design were mainly attributable to the high deformation the foot would experience, thus not providing enough stiffness, and the unevenness of volume deformation along varying angles of contact with respect to the ground.

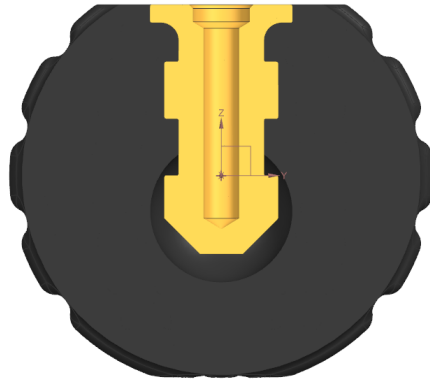


Figure 4.2: Cross section of the first design of the new foot, comprising a spherical control volume and an unchanged pin.

Second Design: Donut

Donut was the name given to the second proposed design. In this case, the issue of too high deformation was addressed, as well as a first attempt at redesigning the pin, which was reshaped and drilled to allow air to pass through. The main issue with this second design was the

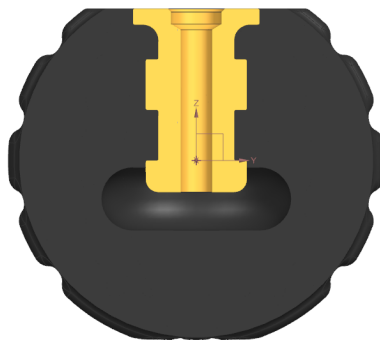


Figure 4.3: Cross section of the second design of the new foot, comprising a toroidal control volume and a first attempt at redesigning the pin.

unevenness of volume deformation throughout different angles of contact, and the low resistance to shear loads along the plane parallel to ground. The results obtained through the numerical simulations performed applying loads to the contact interface between the foot and the ground on the first two designs, and the by then acquired awareness regarding the deformation of the chamber under load, were fundamental in progressing the design phase, with the third design integrating what was good about each of the two designs.

4.2 Foot Design

4.2.3 Third Design: Smile

The third design idea was a mixture of the first two, as it would theoretically provide a higher degree of stiffness to the structure, a constant read along different angles of attack, and a sufficiently high volume deformation even at low loads. This last point was addressed considering as material for the rubber the UPX8400, which was, and currently still is, the rubber of choice for the robot HyQReal's foot. The designs presented in this section were then used as presented

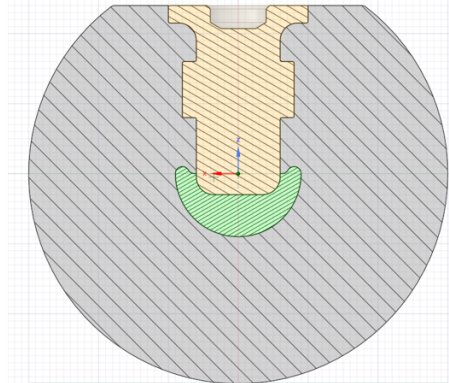


Figure 4.4: Cross section of the refined "smile" design

in the following one, as baselines to guide the design towards a final version that would be then used for the prototyping phase. The next section will be used to highlight the main results obtained through numerical simulations performed using the software Ansys, and how those results were used to assess the final version of the prototype.

4.3 Numerical Analyses: Ansys

The following step in the design phase was to assess the design through numerical simulation; the tool of use was the software Ansys. Ansys is a general-purpose, finite-element modeling package. It finds applications in a heterogeneous variety of mechanical problems, by employing a powerful finite-element modelling package. These problems include static/dynamic, structural analysis, heat transfer, and fluid problems, as well as acoustic and electromagnetic problems. There are two ways to make use of Ansys services. One method is through the GUI. This method follows the conventions of popular Windows and X-Windows-based programs. Another method is to use command files [56]. For the purpose of this thesis the GUI method was the one of choice, although it was later realized that the command file system was more efficient. One of the intents for the future is to implement an algorithm to automate the data management and solving techniques, with the intent to improve its usability in the future.

In order to determine the designed geometries' behaviour under dynamic loads, a rectangular platform was included in the model to simulate the contact surface; this allowed to estimate the foot's behaviour under compression with normal contact to the ground. Before exploring the behaviour of the designed foot, some preliminary simulations were ran by the student, in conjunction with the supervisor Dr. Matteo Villa, to get confident with the software and its components. Therefore, the case of a dome compressing under load and hitting a semisphere was modelled. This preliminary simulation allowed the student to get confident with some advanced techniques later used, such as adaptive remeshing.

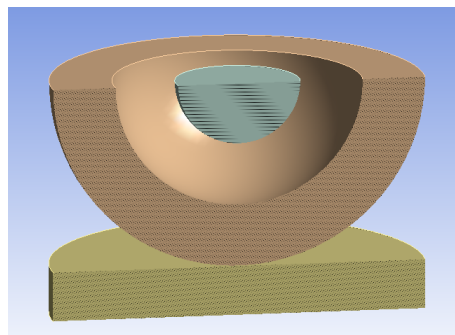


Figure 4.5: Preliminary test model

When gained enough confidence with the tools and methodologies, it was then possible to start playing with the parameters defining the material properties.

It was seeked a model that would deform enough under low loads for the sensor to read a reliable change in pressure, identified as 10% decrease of the initial volume, using the material of the current toe (UPX4800). It was also evaluated the stiffness of the foot structure, as not

4.3 Numerical Analyses: Ansys

to negatively influence the estimation of the foot center position in the state estimator. Finally, it was estimated the theoretical maximum load on the material, and compared with the bulk modulus of the materials not to exceed its limit.

After some failures, a model was defined. Figures 4.6, 4.7, 4.8 highlight the behaviour at varying loads.

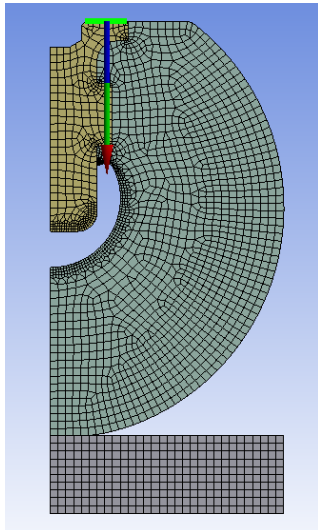


Figure 4.6: Zero load; no deformation.

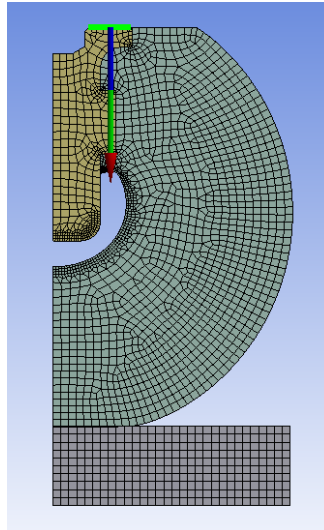


Figure 4.7: 50N normal load; $-10\% \Delta \text{Volume}$.

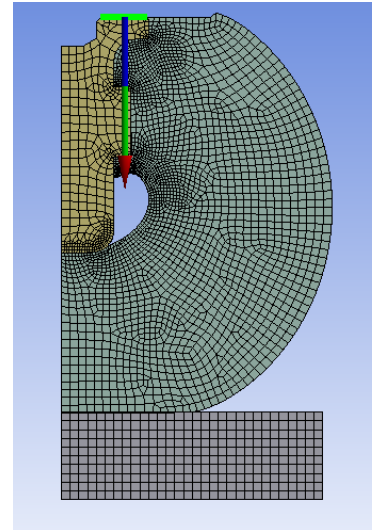


Figure 4.8: 250N normal load; chamber sealed.

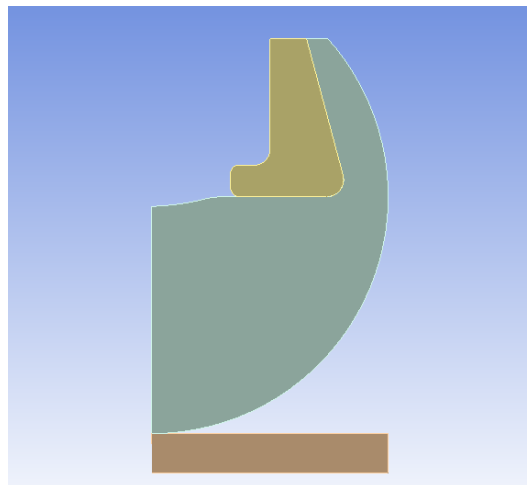


Figure 4.9: Half cross section of one of the discarded designs.

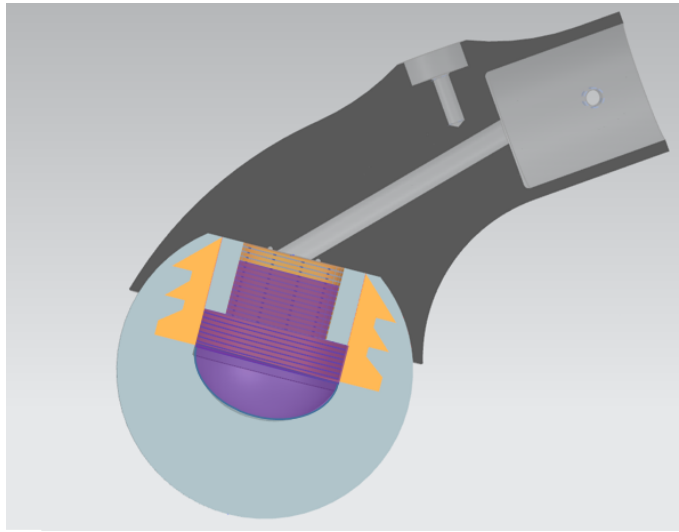


Figure 4.10: Alternative version of the foot cross section

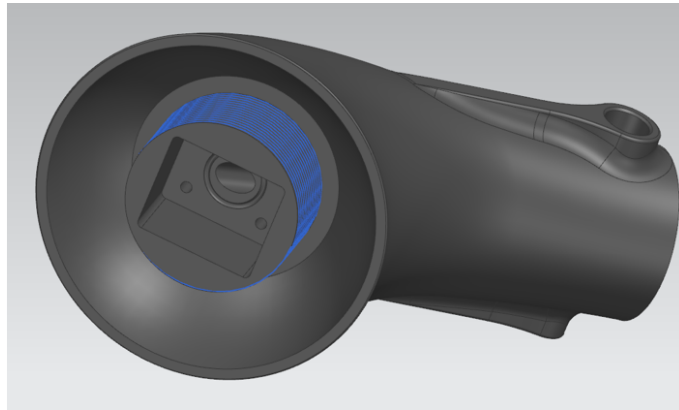


Figure 4.11: Alternative version of the foot, 3D

More or less at the same time during the project development, it was also designed an alternative version to the conservative one presented at the beginning. This version would have required a redesign of the foot structure, but it addressed many of the criticalities inherent in the original foot structure, among which the inability to make an air passage, and the unsatisfied need to embed the sensor in the foot. Some pictures are reported below, which were later tested on Ansys for deformation of the toe rubber structure.

In order to reach a final version of the design for prototyping, the isotropy of the first design and the robustness of the alternative were both taken as inspiration. With this goal in mind, it was developed a model later used for the prototyping phase, and experimental phase. In the final chapter of this thesis it will be addressed how this design is going to be implemented in the robot HyQReal, and considerations on how the design can be further improved in future versions.

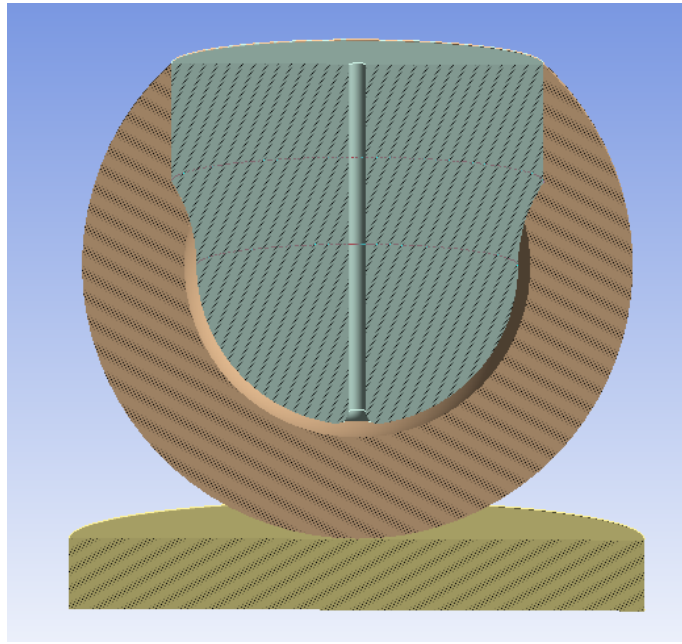


Figure 4.12: 3D cross section of the foot, used as prototype for the experimental phase.

4.3.1 STL export and volume definition

In order to define the air chamber control volume, together with the datasheet provided by the manufacturer [57], it was set up an experimental procedure aiming at roughly estimating the volume decrease required to ensure a reliable read of the pressure sensor, and the effect of the dead (uncompressed) volume on the performance of the sensor. Its description can be found in the first section of Chapter 6. It was concluded that a larger dead volume would have a negative influence on the responsiveness of the sensor. In order to precisely define the dead volume of the chamber, the model was first compacted (single piece), to be then exported in STL format, and then back to Ansys to reverse engineer the volume of air of the undeformed structure. Then, it was done the same thing on the deformed volume; therefore, by some elementary mathematics it was possible to evaluate the volume deformation.

4.3.2 Validation of design and prototyping

Below is reported the model of the final version of the foot, used for experiments. The rubber part of it was 3D printed using the SLA technology in Flexa GM8 and Flexa GM10B, to experimentally evaluate the effect of different shore hardnesses on the sensor's performance, and later the design robustness. The pin used for the prototype was 3D printed in ABS for fast prototyping. In the later stages of the product development, it will be implemented in metal, ceramic or other polymer compounds in order to withstand the high loads provided by the robot HyQReal.



Figure 4.13: STL export of the 3D deformed model.

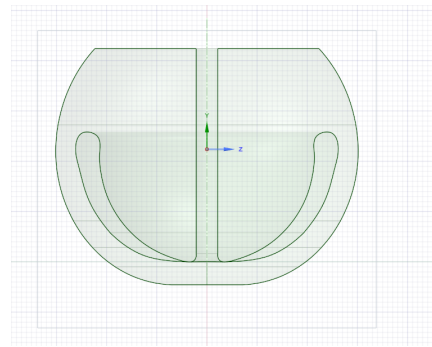


Figure 4.14: Reverse-engineering technique end result.

In alternative, the design proposed earlier as alternative could be exhumed and improved, with the knowledge following these months of work.

As can be seen in Figure 4.15 there is space inside the pin to allow to encase the sensor. This aspect will also be refined for the final version, as to provide higher protection against impact loads, that are usually amongst the most common reason of failure for this kind of sensors.

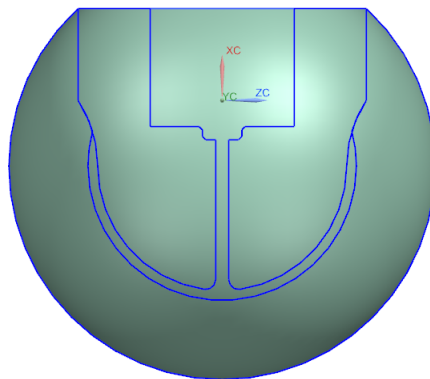


Figure 4.15: Cross section of the foot prototype.

4.4 Alternative foot design

In Figures 4.16, 4.17, 4.18, 4.19, 4.20, 4.21, are reported the results of the numerical simulations performed on the model used for the prototype, highlighting the deformation of the rubber.

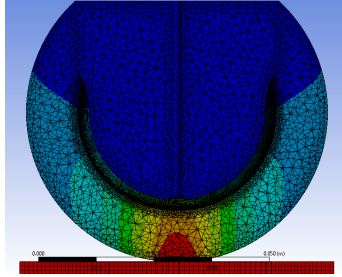


Figure 4.16: No load applied, undeformed shape.

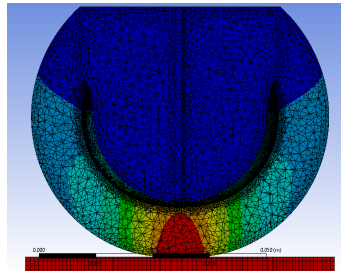


Figure 4.17: 50N load applied; $-10\% \Delta \text{Volume}$.

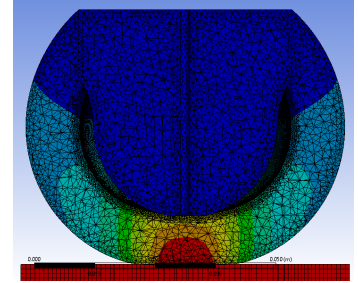


Figure 4.18: 100N load, chamber sealed and $-20\% \Delta \text{Volume}$.

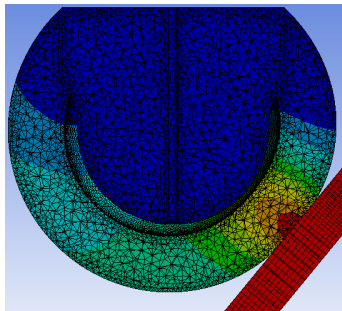


Figure 4.19: 50N load applied at 45° ; $-10\% \Delta \text{Volume}$.

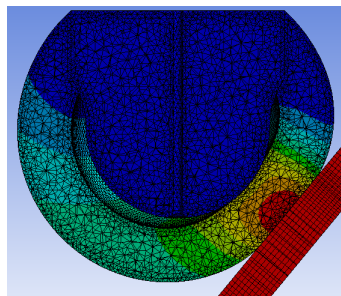


Figure 4.20: 100N load applied at 45° ; $-18\% \Delta \text{Volume}$.

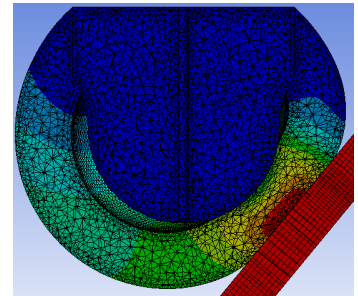


Figure 4.21: 250N load applied at 45° ; $-22\% \Delta \text{Volume}$.

4.4 Alternative foot design

In the picture reported, it is presented an alternative design for the active foot of the robot HyQReal. The design is composite, as it comprises an internal core (in yellow) which could be aluminum, or polymeric, depending on the loads it will experience. The core will be encased in a soft, high viscosity fluid (such as silicon, in grey in the picture) which would dampen the shock loads experienced by the core during impacts. The interface with the rest of the lower leg will be through an interface (in orange), which would also act as control volume for the pressure sensor. The external cover of the foot would be made of elastomeric material (green in the picture), such as vulcanized rubber, to increase the durability and gripping capabilities. The design would have to be validated through experiments, but the smaller control volume would

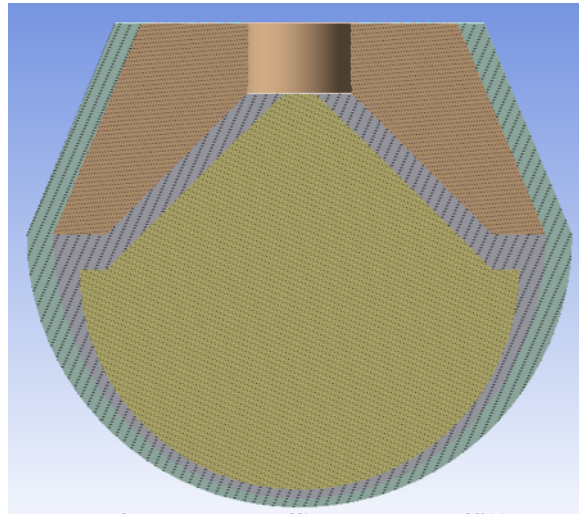


Figure 4.22: Cross section of the alternative proposed foot design.

enhance the effectiveness of the state estimator, and the shear resistance would also be greatly enhanced, compared to the design proposed in this thesis.

4.5 Shin Design

The design of the new shin for the robot HyQReal was driven by the results obtained through the algorithm developed, as explained in detail in chapter 5. In chapter 2 are reported some examples of the state of the art in the field of leg design, from which inspiration will be taken for the prototyping of the new shin for the robot HyQReal. The main idea behind the design itself was to split the single rod configuration in two segments, as to improve the capabilities of the robot to navigate challenging terrains such as stairs. A similar model was implemented in Gazebo and tested for stair climbing for the aforementioned robot, after being exported in suitable format and simplified through the use of the software Blender.

CHAPTER 5

Locomotion and Coding

Chapter 5 puts the attention of the reader on the mathematical and theoretical aspects of legged locomotion, in the specific case of stairs climbing. A script was developed in order to assess the best possible shape of the lower leg to maximize the reachability of the robot. The script is then used to assess the best geometry of the shin for the case of a generic quadruped, and later for the robot HyQReal.

5.1 Motivation

In the past few decades, the great development in the field of robotics has resulted in robots replacing humans in several tasks. Similar progress has also been observed in the development of task oriented robots, for example those used for search and rescue, inspection and delivery. In order to achieve an acceptable level of autonomy in structured and unstructured terrains, a robot must be capable of climbing the stairs (up and down) of a building. Extensive research has been undertaken by many researchers to develop robots with climbing capabilities. These robots are usually categorized into three main groups: tracked, articulated leg and hybrid system. In a track based stair climbing system [58], track belts are used in order to achieve the robot locomotion. Lawn et al. suggested to replace the single track belt system with a double track-belt system, aiming at improving the stability of a step climbing machine [59]. Research was conducted in order to develop a new kind of geometry that is based on a tracked mechanism [60]. Such systems are able to achieve a high degree of controllability and can successfully maneuver on rough terrains and stairs. However, these systems are inherently slower when compared to the wheel based systems. On the other hand, robots that are based on articulate legs [61] tend to be more effective when climbing stairs, although more complex to control. To mix things up even further, researchers are currently working towards the development of hybrid systems, such as wheels with track [62], wheels with articulated legs [63], wheels with legs and legs with wheels -the only limit is once again just the imagination. In this context, the "simple" case of legged robots is analyzed, and the aim is to improve the capabilities and reachability of a quadruped robot performing locomotion over stairs (both up and down), while exploiting novel solutions to improve the maximum step height the quadruped could reach, and to improve the inherent safety of such a system. To do so, a kinematic model of the robot was developed, starting from the general case of a two-link leg. The developed code was used to test the reachability of the robot, exploring various desired points of contact of the foot, at different positions of the base frame (which is located at the center of the torso of the robot). The code was used to test both the shin collision that would occur with the step, and the reachability of the couple of points (if the desired foot position would still lie inside the workspace volume of the robot at the defined position and inclination). The code was then used to assess the best shape to minimize the number of failures (shin collision or foot position outside the workspace). The next step was to update the kinematic model passed to the script to extend the analysis to the robot HyQReal, and to optimize the shape of the lower leg while respecting the geometric and kinematic constraints. It is shown the possibility to extend the use of the script to exploit other parameters,

5.2 Stair Climbing

5.1.1 Workspace

Since it will be used in the following sections, here is provided a definition of the workspace of a generic robotic manipulator. In just a few words, quoting the definition given by Cao et al. , *the workspace of a robot manipulator is defined as the set of points that can be reached by its end-effector* [64]. In this context, the workspace is the volume (or area, in the 2D case) that is reachable by the foot given a certain posture of the robot. It is a function of the geometric parameters defining the robot, and the kinematic limits of the joint, also known as joint space.

5.2 Stair Climbing

While more demanding than level walking, the ability to perform stair climbing locomotion with relative agility is fundamental in order to have robots leaving the laboratories (figuratively and literally) and enter the real world. Stair climbing is one of the main reasons legged locomotion is deeply studied and sought in the first place, as wheeled robot are unable to advance over them, despite numerous efforts and ingenious designs aiming at addressing this problem have been proposed: for instance the tri-wheel robotic platforms.

5.3 Contact Awareness

Unexpected collision are expected to occur commonly in legged robotics during locomotion over unstructured terrain. Although this issue should be ordinarily addressed, often in research it is assumed to have complete and exhaustive awareness of the environment the robot is supposed to transverse, and prefer to focus on motion generation aimed at avoiding collisions altogether. In real world applications, this is rarely the case, as information regarding the topology of the environment might not be available for a number of reason, from malfunctioning sensors to adverse weather conditions. In such cases, the interaction between the environment and the robot is not guaranteed to occur only at the end-effector to ground interface. This is a challenging situation, as most of the advanced control strategies that are used to stabilize the trunk require the exact location and Jacobian of the points of contact [65] [66]. Furthermore, to properly distribute the contact forces, it is also required to have knowledge of the inclination of the contact surface, as well as its frictional properties. Therefore, in order to achieve robust locomotion, as proposed by Barasuol et al. [67], it is key to detect unexpected collisions to then use them as feedback in order to stabilize the trunk controller. Several research attempts have been developed in order to find methodologies aiming at detecting or estimating the location of

points of contact along the robot structure: to mention a few, Del Prete et al. proposed to use a 6-axis force/torque sensor, in conjunction with a compliant skin incorporating a distributed pressure sensor, based on capacitive technology, in order to estimate the contact location, on the robotic platform iCub developed at IIT [68]. Ivaldi et al. proposed a way to retrieve force feedback from existing robots not directly equipped with joint torque sensors (JTS), by using three different sets of sensors: inertial, force/torque and tactile. The presented technique provided a complete perceptual depiction of the intrinsic dynamics of the robot, as well as a representation of the interaction forces arising due to external contacts [69]. Despite the promising potential of using distributed pressure sensors as an artificial skin, its use up to now is limited to tactile low-force applications, and they are not designed to handle high impact forces; therefore limiting their application in shin collision detection. Other ways to detect robot collision make use of estimation, as for example proposed by de Luca et al. in [70]. In this latter research topic, they proposed to handle a collision at a generic point along the robot as a fault of its actuating system. Once contact is detected, it would then be possible to switch to a suitably defined hybrid force/motion controller enabling to keep the contact, while sliding on the obstacle, and to regulate the interaction force. It is to be noted that this approach has been only tested in simulation for a two-link planar robot. The advantage of using an estimation based technique to localize contact is that it is only required to use proprioceptive measurements, without the need of including additional force sensors. In general, given also the high complexity of the estimation algorithms, it is common in these approaches to fail to determine the exact contact location, especially when dealing with the most distant links interactions. Extending the analysis to quadruped robots, shin collision are usually unsought circumstances, as they can cause the robot to get stuck during locomotion. This situation is worsened in case of *blind* locomotion, a condition in which the robot is unable to properly evaluate the environment it is navigating within. In the next sections it is shown the rationale followed in order to minimize the possibility of shin collision by acting on the geometrical structure of the lower leg, and at the end of the chapter it is presented a novel solution aiming at improving even further this condition.

5.4 Code Development

The code developed, in conjunction with the supervisor Dr. Victor Barasuol, is presented in this and the following sections. It is highlighted how the concept of modularity was sought, and how the functions making up the main structure of the code were developed. The script functions as follows: at first, it retrieves the data related to the kinematic structure of the robot,

5.4 Code Development

the parameters defining the stairs, and the task parameters, which are used to define the step length, the height of the robot.

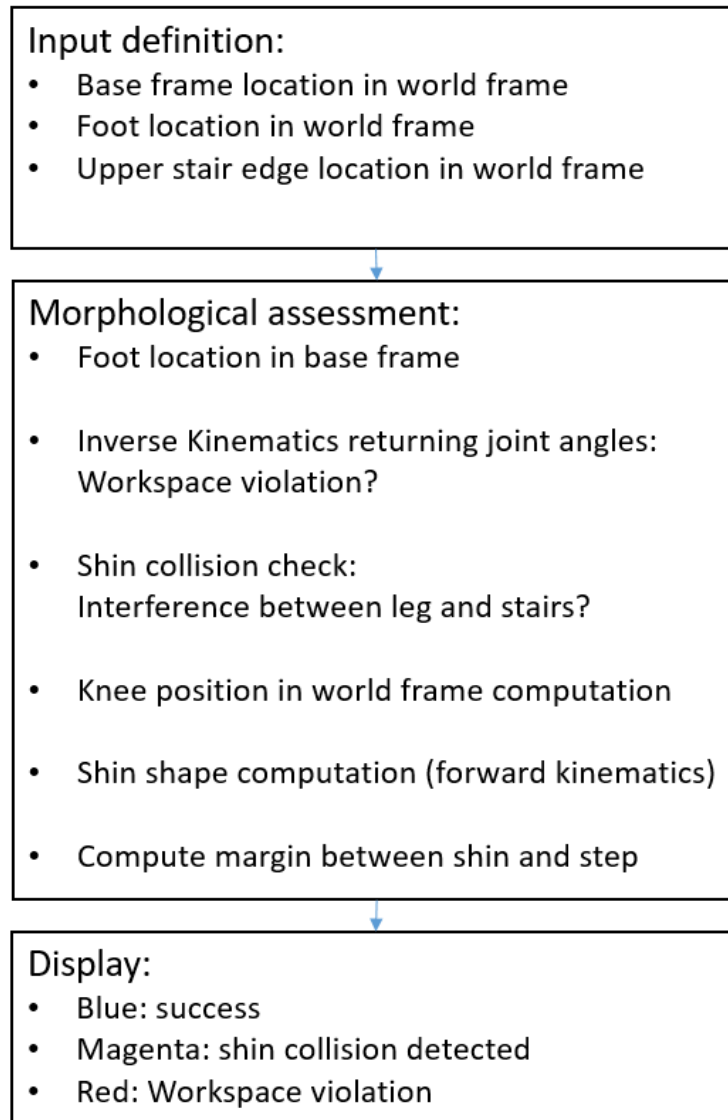


Figure 5.1: Structure of the code

5.4.1 Input Definition

The first piece of analysis is dedicated to the definition of the parameters comprising the kinematic and geometric properties of the robot and the stairs, as well as the parameters defining the task. The parameters are defined as structures divided in: Kinematic definition of the robot (K), Stair parameters (S), and task parameters (T). It will be shown in the following sections how changing the values and dimensions of the structure does not affect the performance of the algorithm, thus improving reusability.

Kinematic Model

Below are reported the parameters used to rigorously define the kinematic structure of the quadruped robot.

K structure description

t_l Defines half of the length of the torso length, from the base frame (located at the center of the trunk) to the position of the hip joint.

l1 Defines the length of the upper segment of the leg of the robot (the thigh), from the hip location to the knee location.

l2 Defines the length of the lower segment of the leg of the robot (the shin), from the knee joint position to the end-effector location. The shin is then divided in two segments, which will be modified to improve the capability to avoid shin collision through the use of the developed script.

l2p Defines the length of the upper segment comprising the new design of the shin, from the knee joint location to the point of bending.

beta Defines the angle of bending of the two segments comprising the newly designed shin.

$q1_{min}$ Defines the minimum angle of the HFE joint.

$q1_{max}$ Defines the maximum angle of the HFE joint.

$q2_{min}$ Defines the minimum angle of the KFE joint.

$q2_{max}$ Defines the maximum angle of the KFE joint.

yaw Defines the yaw angle of the robot, with respect to the ground plane.

kneebend Defines the orientation of the knee: 1 if it is bent backwards (KBB), 0 if bent forward (KBF).

S structure definition

pps Defines the number of points comprising each stair step.

rise Defines the height of the step.

go Defines the length of the step.

n Defines the number of steps comprising the stair.

T structure definition

step length Defines the position of the foot with respect to the hip joint. It is the parameter it is iterated over in order to evaluate the kinematic assessment.

robot height Defines the height of the robot base frame with respect to the step directly underneath it.

delta pitch Defines the variation of torso inclination with respect to the locomotion line.

swing margin Defines the minimum distance between the lower leg and the step. It is used to assess the radial dimension of the leg (diameter of the tube in the case of HyQReal).

Once the kinematic properties are defined, the relevant quantities can be extrapolated to be then used in the morphological assessment. The first step is to define the locomotion line along which the robot trunk will move and to generate the stairs. The first assumption is that the robot trunk is parallel to the hypotenuse of a step. In order to define the line equation,

$$y = m * x + q \quad (5.1)$$

at first the angle is computed as

$$m = \tan(\text{rise/go}) \quad (5.2)$$

The distance to the origin (q) is then defined using the robot height parameter, under the assumption that the stairs initial point is located at the origin. An initial base frame location is then defined. In the context of stairs descent, the base frame location is defined at first at the top of the stairs. Once the base frame location is fixed, the first desired foot location is computed, such as:

$$x_f = x_b - (\text{step_length}/2 + \text{torso_length}/2) * \cos(\text{atan}(\text{rise/go}))$$

the z position of the foot desired location is computed according to the steps geometry. It is then retrieved the position of the stair edge right above the desired foot location, as it will be used in the following section. To summarize the first part of the script, related to the inputs definition, a series of structures is passed a priori to the algorithm, a base frame location is then computed starting from the knowledge of the step parameters, and a vector U is returned. The vector contains the base frame location (x and z), the desired foot contact location (x and z), the location of the step edge right above the foot desired location, and the pitch angle of the

robot (the angle the trunk makes with respect to the ground plane). All the locations are given in the world frame.

5.4.2 Kinematic Assessment

The second part of the algorithm aims at evaluating the feasibility of reaching the desired foot location with the robot positioned as defined through the base frame location and the pitch angle. The first manipulation of the inputs is to retrieve the desired foot location in the base frame. To do so, rotation matrices are used to compute the relative position, such as:

$$R_y(\theta) = \begin{bmatrix} \cos(\theta) & 0 & -\sin(\theta) \\ 0 & 1 & 0 \\ \sin(\theta) & 0 & \cos(\theta) \end{bmatrix}$$

$$R_z(\psi) = \begin{bmatrix} \cos(\psi) & -\sin(\psi) & 0 \\ \sin(\psi) & \cos(\psi) & 0 \\ 0 & 0 & 1 \end{bmatrix}$$

$$R_b^w = R_y(\theta) * R_z(\psi) \tag{5.3}$$

The foot location in the base frame is then computed as:

$$(x_f, y_f, z_f)_b = R_b^w * (X_f - X_b)_w \tag{5.4}$$

Inverse Kinematics Algorithm

The next step is to retrieve the joint angles required to generate the kinematic chain. This also serves as a first check, since, if a solution is not found, then the foot location is outside of the workspace of the robot in the current configuration.

The function works as follows: at first the distance between the HFE joint and the desired foot position is computed as

$$x_f^{hfe} = x_f^b - torso_length/2 \tag{5.5}$$

$$p_f^{hfe} = \sqrt{(x_f^{hfe})^2 + (z_f^b)^2} \tag{5.6}$$

Then the maximum and minimum p_f^{hfe} allowed according to the maximum and minimum knee joint angles are computed. The computation is different in case the knee is backward (KBB) or forward (KBF).

5.4 Code Development

If KBB:

$$p_{hfe,min} = \sqrt{l1^2 + l2^2 - 2 * l1 * l2 * \cos(\pi + q2,min)} \quad (5.7)$$

$$p_{hfe,max} = \sqrt{l1^2 + l2^2 - 2 * l1 * l2 * \cos(\pi + q2,max)} \quad (5.8)$$

If KBF:

$$p_{hfe,min} = \sqrt{l1^2 + l2^2 - 2 * l1 * l2 * \cos(\pi - q2,min)} \quad (5.9)$$

$$p_{hfe,max} = \sqrt{l1^2 + l2^2 - 2 * l1 * l2 * \cos(\pi - q2,max)} \quad (5.10)$$

The next steps is to assign the leg extension, and to compute the corresponding knee joint angle. Equation 5.11 is described in the book Robotics by Bruno Siciliano [71], and it allows to compute the angles of a two link planar arm given the geometric parameters, the orientation of bending, and the position of the end-effector with respect to the base frame (HFE in this context). The angle between the upper and the lower leg segments is computed as:

$$\alpha = \arccos((l1^2 + l2^2 - (p_f^{hfe})^2)/(2 * l1 * l2)) \quad (5.11)$$

If KBB:

$$q2 = -\pi + \alpha \quad (5.12)$$

If KBF:

$$q2 = \pi - \alpha \quad (5.13)$$

Then, the angle between the line that connects the hip to the foot and the upper leg link is computed as:

$$\beta = \arccos(((p_f^{hfe})^2 + l1^2 + l2^2)/(2 * l1 * p_f^{hfe})) \quad (5.14)$$

The next step is to compute the angle between the line that connects the candidate foot position to the azimuthal line passing through the hip joint as:

$$\gamma = \arctan(x_f^{hfe}/z_f^b) \quad (5.15)$$

The hip joint angle is finally computed as:

If KBB:

$$q1 = \gamma + \beta \quad (5.16)$$

If KBF:

$$q_1 = \gamma - \beta \tag{5.17}$$

The final step is to check whether the computed angles are within the kinematic limits of the robot, defined in the K structure. If they are, a positive flag is returned as output from the function together with the angles computed; if they are not, a negative flag is returned, together with the maximum (in case the computed angle is above the maximum limit) or the minimum (if below the minimum limit).

Shin Collision Check

The following portion of the algorithm is used to check whether a collision occurs at the shin level with the step. To do so, the first step is to retrieve the **foot** position (which is different from the desired one computed in the input definition, as it considers the actual joint angles) and the **knee** position in the world frame. The foot position is computed exploiting the kinematic chain that links the base frame to the foot joint. A forward kinematics (FK) equation, used to retrieve such position is then presented, with the previous knowledge of the base position in the world frame, and the orientation of the torso with respect to the ground:

$$x_{hfe} = x_b - t_l/2 * \cos(\theta) \tag{5.18}$$

$$z_{hfe} = z_b - t_l/2 * \sin(\theta) \tag{5.19}$$

$$x_k = x_{hfe} + l1 * \cos(\theta + q_1 - \pi/2) \tag{5.20}$$

$$z_k = z_{hfe} + l1 * \sin(\theta + q_1 - \pi/2) \tag{5.21}$$

$$x_f = x_k + l2 * \cos(\theta + q_1 + q_2 - \pi/2) \tag{5.22}$$

$$z_f = z_k + l2 * \sin(\theta + q_1 + q_2 - \pi/2) \tag{5.23}$$

Then these positions, in conjunction with the shin bending angle, are used to describe the two segments comprising the shin.

5.5 Usage: Shin Shape Optimization for a generic Quadruped

For the upper segment:

$$a_1 = (z_k - z_f)/(x_k - x_f) \quad (5.24)$$

$$\alpha = \pi - \beta - \arcsin(\sin(\beta) * l2p/l2) \quad (5.25)$$

$$a_{s1} = \tan(\arctan(a_1) - \alpha) \quad (5.26)$$

$$b_{s1} = z_k - a_{s1} * x_k \quad (5.27)$$

For the lower segment:

$$a_{s2} = \tan(\arctan(a_{s1}) - \beta) \quad (5.28)$$

$$b_{s2} = z_f - a_{s2} * x_f \quad (5.29)$$

The line equations are then used to compute the distance to the upper step edge, using the equation:

$$d = (a_{sn} * x_e - z_e + b_{sn})/\sqrt{a_{sn}^2 + b_{sn}^2} \quad (5.30)$$

$\forall n \in 1,2$ If the distance of at least one of the two segments is less than a predefined margin, there is shin collision occurring, and it is returned a negative flag as output. In contrast, in case distances are above the threshold, it is returned a positive flag.

Posture Maker Function

The last portion of the morphological assessment part of the script is dedicated to create a vector containing the position points of each joint comprising the robot analyzed. The kinematic chain is exploited, and a forward kinematic algorithm is then developed. The vector will then be passed to the output function, together with the flags, to determine the condition that has occurred (points couple successful, shin collision detected, workspace limit not respected). For each of these situations, a colour code is given to have a visual representation of the occurrence.

5.4.3 Output Function

The output function receives as input the posture vector described in the previous section.

5.5 Usage: Shin Shape Optimization for a generic Quadruped

Figure 5.2 reports some snapshots of the output function of the script, as developed for Matlab environment. The red +s on top represent the locomotion line (spaced by a step length), with the black * moving along the locomotion line indicating the base frame location. The blue *s indicate

the stairs, with the edges highlighted as light blue +s. The red \star indicate the foot position. In this earlier version of the script, there was no visual distinction between the workspace violation (upper left) and the shin collision (lower left); this, as well as returning a configuration physically possible for the robot, were addressed in later and more refined versions of the script.

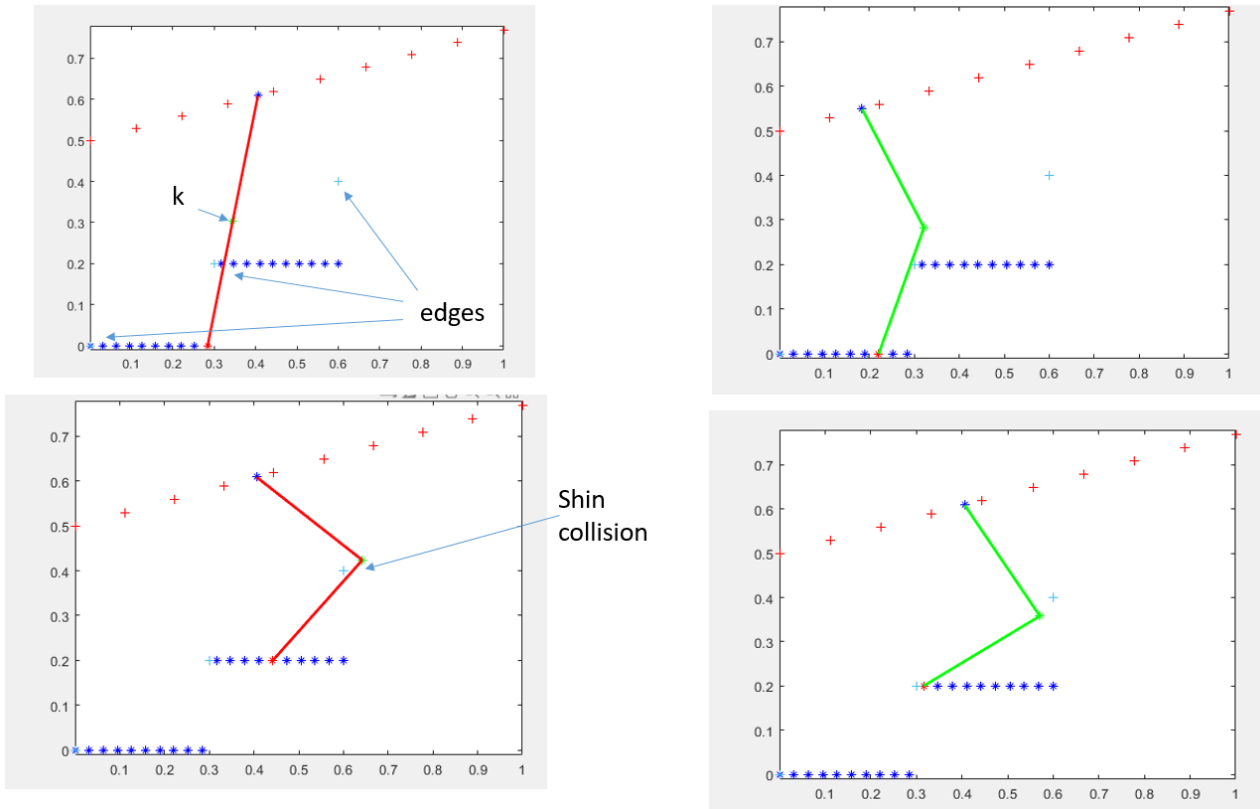


Figure 5.2: Script usage: generic leg output

5.6 Usage: Shin Shape Optimization

The first usage of the script was used to evaluate the optimal shape of the shin, with the goal of minimizing the number of failures occurring due to either shin collision or workspace not respected. In order to obtain a meaningful number of data points, a double iteration was developed. The script structure is defined as follows:

- store initial configuration of the lower leg as the most successful one.
- for -base frame location- moving along the locomotion line;
- for desired foot position moving along the interval \pm half of the step length;

5.6 Usage: Shin Shape Optimization

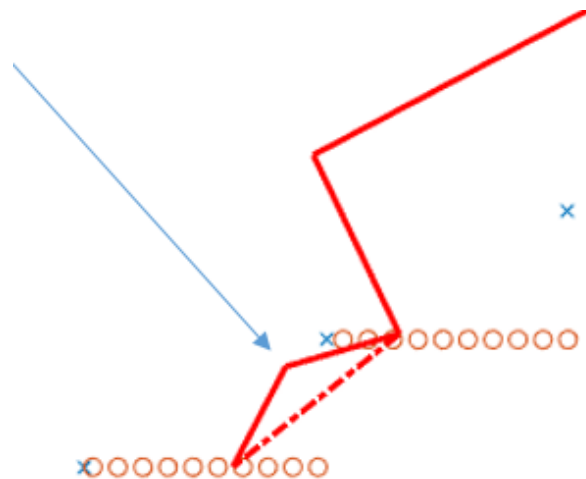


Figure 5.3: Highlight of the shin bending, indicated by the blue arrow.

- compute input vector;
- assess morphology;
- display and return exit condition (passed or failed);
- save the failure conditions;
- act on the lower leg parameters;
- if the number of failures in the current configuration is lower than the most successful one, save the current configuration as the most successful one;
- repeat for all possible leg configurations, while respecting the geometric constraints defined a priori.

In the above picture, a snippet taken during the execution of the shin shape optimizer is shown, in which are highlighted the two segments comprising the lower leg, with the dashed line being kept fixed in length as an additional constraint. Below is reported the result obtained running the script on the standard IIT stairs, defined as 16 cm high (rise) and 20 cm long (go). In figures 5.7 and 5.8 are reported the execution outputs related to the baseline (single link shin), and the optimized shape. The baseline returned a success rate of 25%, while the optimized shape returned a success rate of 56%, thus succeeding in reaching the desired foot position **2.25** times more often than the basic shape.

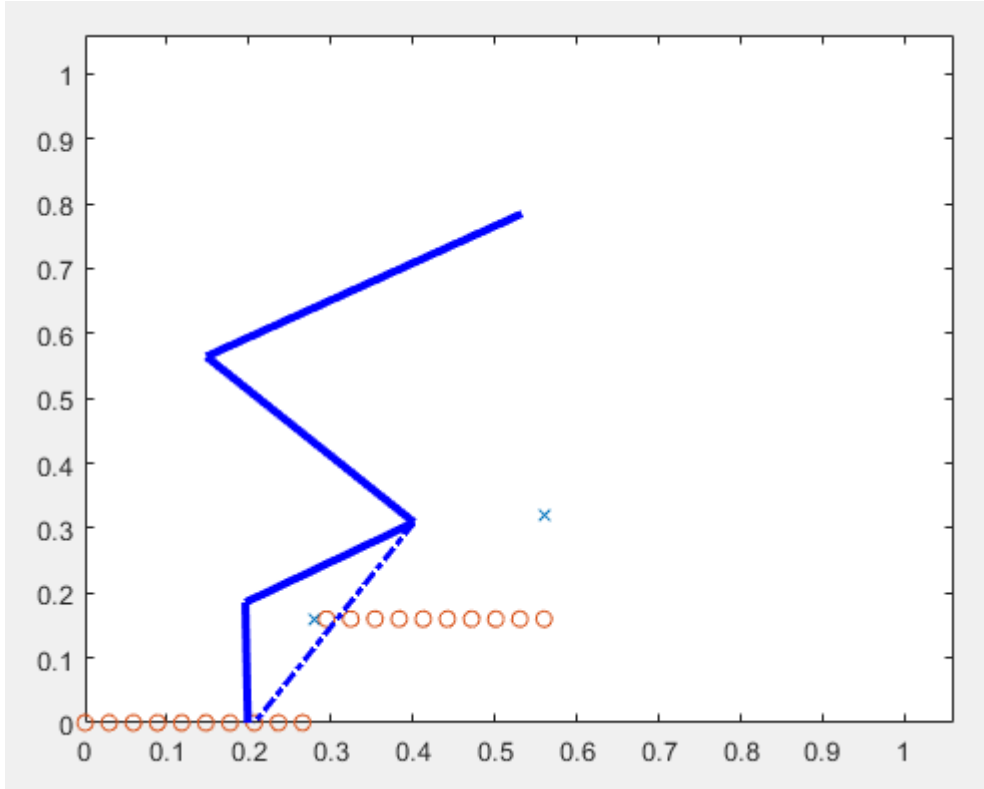


Figure 5.4: Result of the analysis: best shape for generic quadruped

The next step in the analysis is the redefinition of the K parameters, to assess the best shape for the robot HyQReal. To do so, the lower leg parameters were completely redefined to take into account the geometry of the leg, as well as the knee and the foot. The kinematic limits of the joints had to be then redefined accordingly. In order to rigorously describe the lower limb of the robot HyQReal, the lower leg was defined as a chain comprising four links: one for the knee, two describing the shape of the shin, and one for the foot, named (knee to foot) a_1 , a_2 , a_3 , a_4 . In order to compute a_3 and its angle of bending, through the knowledge of segments a_1 , a_2 , a_4 and the relative angles, the Jacobian of the chain was exploited. At first, the symbolic expressions relative to the end point were computed: by solving the kinematic chain, it was obtained:

$$x = a_1 * \cos(\alpha_1) + a_2 * \cos(\alpha_1 + \alpha_2) + a_3 * \cos(\alpha_1 + \alpha_2 + \alpha_3) + a_4 * \cos(\alpha_1 + \alpha_2 + \alpha_3 + \alpha_4); \quad (5.31)$$

$$z = a_1 * \sin(\alpha_1) + a_2 * \sin(\alpha_1 + \alpha_2) + a_3 * \sin(\alpha_1 + \alpha_2 + \alpha_3) + a_4 * \sin(\alpha_1 + \alpha_2 + \alpha_3 + \alpha_4); \quad (5.32)$$

The jacobian was then constructed solving the partial derivatives, computed as follows:

$$\delta x / \delta a_3 = \cos(\alpha_1 + \alpha_2 + \alpha_3) \quad (5.33)$$

5.6 Usage: Shin Shape Optimization

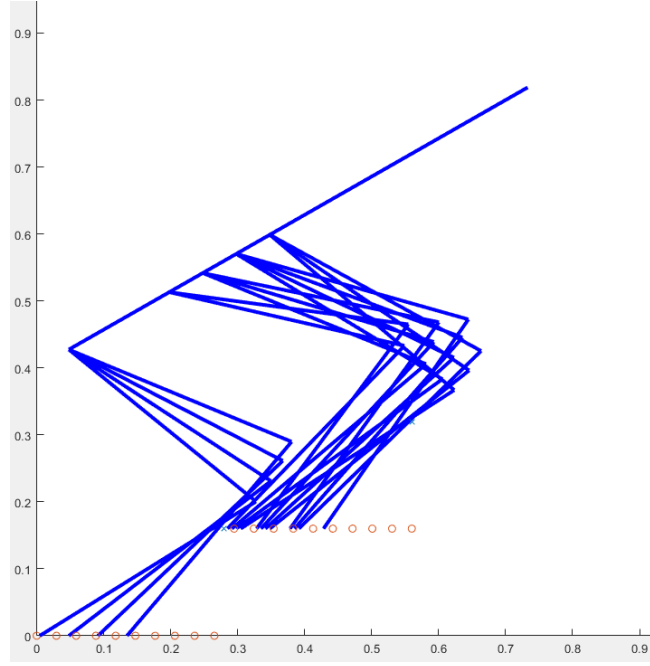


Figure 5.5: Script output display of successful trials, for a generic leg configuration

$$\delta z / \delta a_3 = \sin(\alpha_1 + \alpha_2) + \alpha_3 \quad (5.34)$$

$$\delta x / \delta \alpha_3 = -a_3 * \sin(\alpha_1 + \alpha_2) + \alpha_3 - a_4 * \sin(\alpha_1 + \alpha_2) + \alpha_3 + \alpha_4 \quad (5.35)$$

$$\delta z / \delta \alpha_3 = a_3 * \cos(\alpha_1 + \alpha_2) + \alpha_3 + a_4 * \cos(\alpha_1 + \alpha_2) + \alpha_3 + \alpha_4 \quad (5.36)$$

$$J = \begin{bmatrix} \delta x / \delta a_3 & \delta x / \delta \alpha_3 \\ \delta z / \delta a_3 & \delta z / \delta \alpha_3 \end{bmatrix}$$

Changes had to be made in some of the functions to ensure the correctness of the results obtained. For instance, the function checking the shin collision had to be rewritten to check multiple segments, and the posture maker too. The results of this analysis are shown in the Figures 5.7 and 5.8. The proposed design is in line with the specifications regarding clearance and maximum bend of the shin.

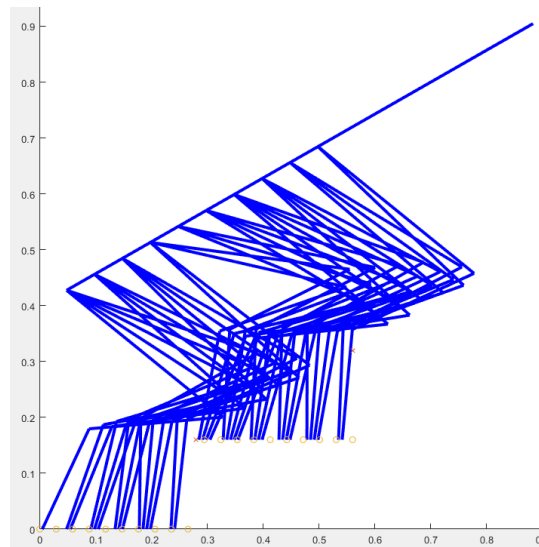


Figure 5.6: Script output display of successful trials, after leg shape was optimized

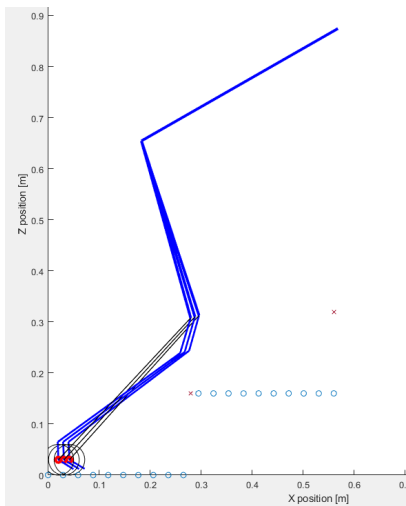


Figure 5.7: Current lower leg version of the robot HyQReal.

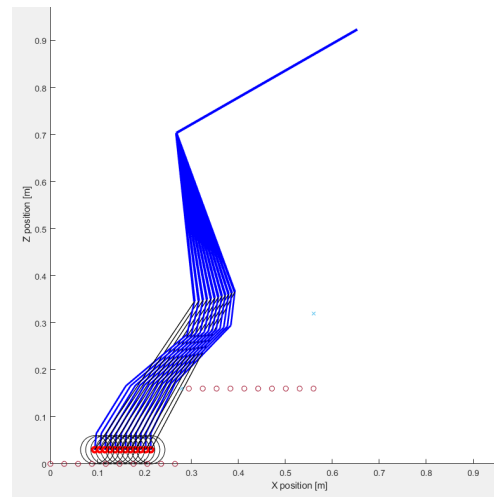


Figure 5.8: Proposed design of the lower leg for the robot HyQReal.

Experiments

The experiments presented in this chapter were designed to validate the hypothesis of using the newly designed foot to improve the robot's sensing capabilities while reducing the threshold at which the contact is sensed. In the current version of the robot, this threshold is kept at 50 N, as reducing it to a lower value would cause unwanted false positives to be estimated, due to the inertia of the leg. The target of this design is therefore to reduce this threshold, to a value of 25 N. It is although proved, through experiments reported in this chapter, that using this design could lower the threshold to 10 N, a 500% reduction from the original value. The experiments were divided into three sections: at first, the design was validated using static loads to have a first impression of the readings coming from the pressure sensor. Data was acquired using an Arduino board, and fixed weights applied normal to the ground to the foot. Then the analysis was extended, performing the same static test on a Kistler force plate to relate the load applied to the pressure read and have a first approximation of the sensor's response time. The experiments were concluded with a dynamic test on the test rig available in the laboratory. In this last phase, the foot was mounted on the lower leg, and dynamic loads comparable to those experienced during regular use were applied. This provided a deeper understanding of the dynamic behavior of the sensor, as various loads were applied, and the swing phase was set at various frequencies. Different points of contact between the foot and the ground were also considered throughout the stages of validation.

6.1 List of Materials

Sensor The sensor chosen was the NXP MPL3115. The choice was motivated by the high sensitivity the sensor provided, the ease of connection and data read through the I^2C communication protocol integrated within the PCB the sensor was mounted on out-of-the-box, and the high degree of overloading allowable (up to 600 % FSO), which was significantly higher than the comparatively priced alternatives.

Toe Prototype Two versions were made, with varying shore hardness to assess the most promising one. Both versions were 3D printed at the IIT workshop using the SLA technology. The materials used were Flexa GM08 (shore hardness 25D) and Flexa GM10B (shore hardness 50A).

Pin Prototype The pin that provides internal rigidity to the foot and housing to the sensor was 3D printed using FDM technology, and the material was ABS. Since the FDM technology does not ensure absolute sealing, the pin was post-processed by the student using a layer of nail polish.

Sealants: -Silicon In order to ensure that the control volume was as close as possible to the theoretical one, the sensor was fixed within the pin using two layers of sealants: at first, a silicon based compound was laid at the contact surface between the sensor and the pin. This also ensured that the layer of epoxy would not ooze at unwanted locations, with the possibility of destroying the sensor itself, while also allowing a minimum degree of compliance to the structure, considering that the most common reason for rupture of sensors is shock load.

-Epoxy Resin A layer of epoxy resin was poured on top of the sensor to ensure an airtight seal of the control volume. Another layer was used to bond the pin to the toe (see pictures below). The resin was mixed and left to cure overnight, according to the time specified in the datasheet.

-Super Glue Superglue was used, together with the silicon compound, to provide a final layer of sealing of the cables and the external interface pin-toe.

Force Plate The force plate used to run the experiments on the lower leg test rig was the type 9260AA from Kistler. According to the datasheet, it provides a shallow threshold (<250mN) while allowing a high degree of linearity (<0.5% FSO), high overload protection, and a sensitivity range of ≈ 19 mV/N. The sensitivity was tested and confirmed before starting the experiments.

Data Acquisition System The DAQ used, in conjunction with the force plate, was the

6.2 Foot Prototyping

DT9812 from National Instruments. It provided analog inputs (8 multiplexed) along with analog output and digital functions. For the use in the experiments, the single digital output port (USB), together with the software QuickDAQ, was used to perform data collection.

Lower Leg Test Rig A testing fixture developed in the DLS lab at IIT to test, calibrate, and validate the lower leg components, starting from the ISA going all the way down to the foot.

ISA Integrated Smart Actuator: See Chapter 2 for more details regarding the Integrated Smart Actuator.

Wooden blocks Cubic and parallelepiped blocks were necessary to raise the force plate, in order to use it in conjunction with the test bench. At first they were meant to be made of steel, but as there were delays in the order it was opted to use beech wood ones for the experiments presented in this chapter. Two different sizes were purchased to assess the load applied at different foot contact points. Beech was the wood of choice as it provides good mechanical properties and does not deteriorate easily.

Coffee scoop The best companion I could ask for during the experimental phase. Numerous were the applications in everyday work, from relieving stress to being used as a brush to lay silicon and epoxy resin to seal the prototypes. A true lifesaver.

6.2 Foot Prototyping

The foot prototype was made of rubber (external surface, more on that on Chapter 4), whereas the pin was made of ABS (aluminum in the production phase). The sensor was encased within the pin and fixed using a silicon compound, to be then covered by a layer of epoxy resin in order to ensure the hermetic seal of the chamber. Figure 6.1 depicts the sealed chamber after one night of curing.

In order to provide an hermetic seal of the interface rubber/abs, a layer of epoxy resin was deposited to the face of contact between the pin and the rubber toe. The resin was left to cure overnight, as per datasheet specifications. The day after, the cap was added to add the ability connect the foot to the robot leg structure. Cabling, soldering, and connections, were then done under the supervision of senior technician Salvatore Casella. Below is reported a picture of the first prototype completed, with a shore hardness of 25A. After some tests, and another prototype being made with harder rubber (shore 50D), it was concluded that the latter would be the better

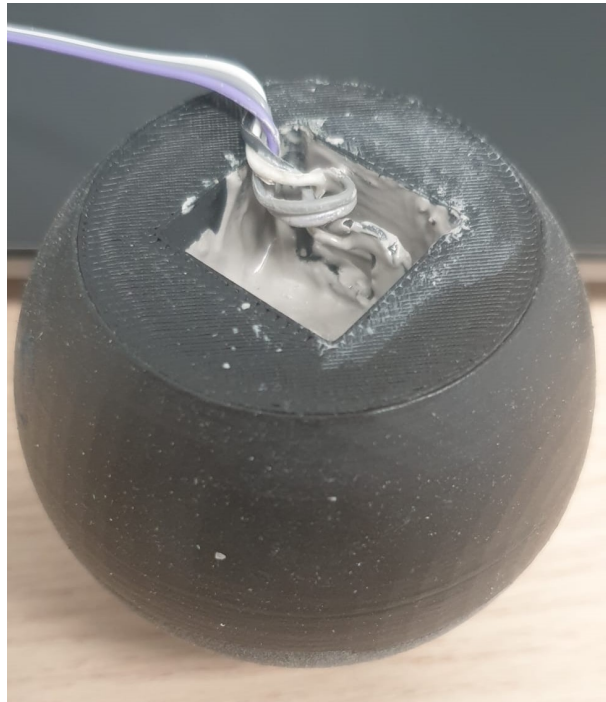


Figure 6.1: Highlight of the sensor chamber, encapsulated in epoxy resin

candidate for the experiments, as additional measures to ensure the sealing of the chamber were taken, and the preliminary tests proved to be more reliable and successful than the first one.

6.3 Data Collection

Data had to be collected from multiple sources, sometimes simultaneously during the experiments. In order to gather data coming from the pressure sensor, a simple circuit for signal acquisition was developed using an Arduino UNO board as the PCB responsible for handling the dataflow. Data was then gathered on the PC by means of a script, written by the student based on the baseline provided by the manufacturer. In order to save data, a script was developed to produce a csv file comprising the pressure read and the global time. This simplified the data handling, and reduced the possibility of human error as the process was automatized.

To gather data from the force plate, the DT9812 DAQ board was used, in conjunction with the software QuickDAQ. Through this software, and a modified version of the script written for continuous data acquisition of the pressure sensor through Arduino, it was implemented a trigger function comprising a pushbutton to which both acquisition boards were connected, and a common ground. A schematic of the circuit just presented is shown in the figure below.

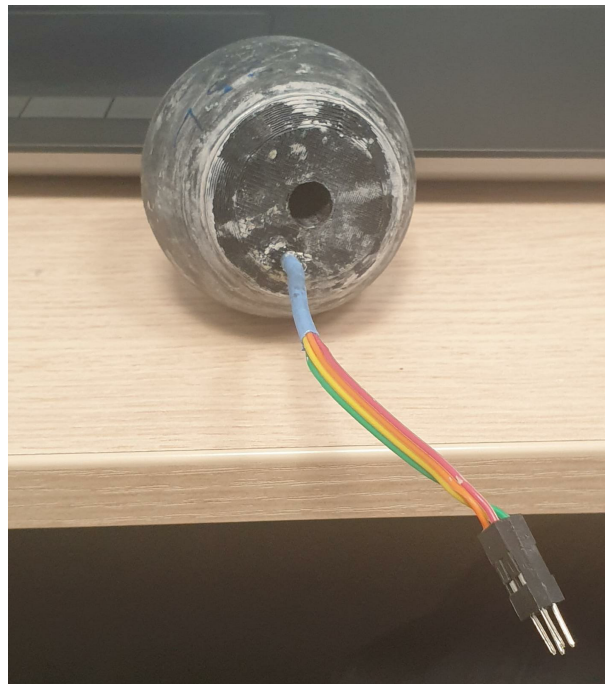


Figure 6.2: First prototype of the foot assembly

6.4 Sensor Testing

In order to test the behavior of the sensor, a testing feature was designed and used in conjunction with a syringe for the preliminary tests on the sensor. Below is reported a picture taken during one of this preliminary tests, used to assess the effect of varying dead volumes on the sensor response (both in terms of peak and response speed). At the end of these tests, it was concluded that the sensor's response speed was around 60 ms, and that the dead volume had no effect in the response speed, but the pressure read with larger initial volume was less reliable than that of a smaller dead volume. Sensor responsiveness was more rigorously measured in the following sections presented in this chapter, as more confidence with the testing equipment was acquired and the prototypes finalized.

6.5 Force Plate Calibration and Prototype Preliminary Tests

In order to have a preliminary estimation of the sensor capabilities, and to test the setup of the force plate, preliminary tests were carried out by applying fixed loads to each of the piezo cells of the force plate. Once the linearity in readings was assessed it was elaborated the sensitivity of the force plate, in order to convert the output voltage read into Newtons. The result, at FSO (full scale output) of 250N it was estimated a sensitivity of 18.95 mV/N, in line with data

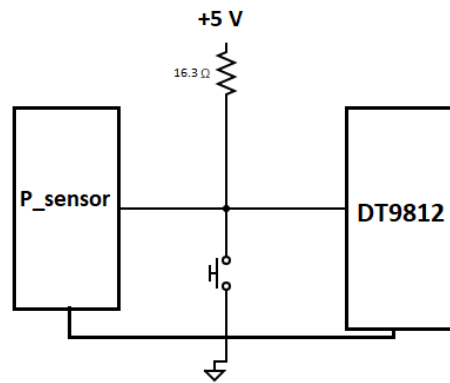


Figure 6.3: Schematics for simultaneous read

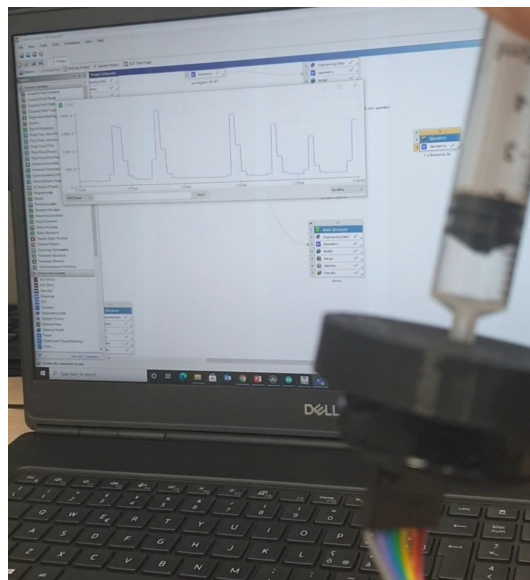


Figure 6.4: Picture taken during the preliminary dead volume test of the sensor

provided in the datasheet.

To test the responsiveness of the sensor, and to assess if there was air leakage in the control volume chamber, preliminary tests were carried out on the foot. Fixed loads were applied on top, and data coming from the sensor was read through the Arduino. This allowed to improve the first prototype's design, and the second proved to be way more reliable. It was noticed, during this phase, that a smaller diameter of the needle connecting the control volume to the sensor provided a more repeatable read, and a substantial improve in keeping the pressure constant by keeping the load applied. This property will be further explored in future works, by also exploring the effect of varying other needle geometric parameters, such as length of the tube. Below are reported screenshots of the raw output coming from the Arduino, of the first and

6.5 Force Plate Calibration and Prototype Preliminary Tests

second prototype; the same load was applied to both feet during this particular test. As can be clearly seen, the first one fails significantly in maintaining a constant pressure. The second is not perfect either though, currently this is being assessed by studying the effects of pressure waves propagating through an air medium, the results of which will be assessed in future works.

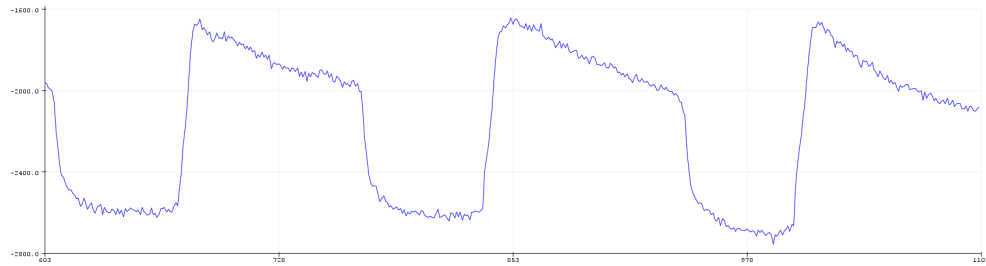


Figure 6.5: First prototype dynamic behaviour as load is applied



Figure 6.6: Second prototype dynamic behaviour as load is applied

6.5.1 Troubleshooting

As commonly occurs in the research field, the experimental phase was not always a, forgive the slang terminology, a smooth ride.

There was mainly a problem that affected the experiments workflow, and it was related to the laboratory table and the ISA. As the new ISA (the one used for the next experiments) was mounted on the test bench, it failed to provide a consistent reading, and it failed continuously without returning any error flag. As the situation was novel even for the researchers in the lab, some time was spent by the student and supervisor Dr. Victor Barasuol trying to assess the issue. It was concluded that the problem was related to the grounding of some components located in that side of the lab, and that affected the signal in the CANopen bus. This issue was solved by grounding the hydraulic hoses to the power line's grid ground. The same issue was later found on the force plate's acquisition system, and was solved by connecting the ground in the input analog channels to the ground of the output channel which, in turns, is connected to the PC ground through the USB, and then eventually to the power grid.

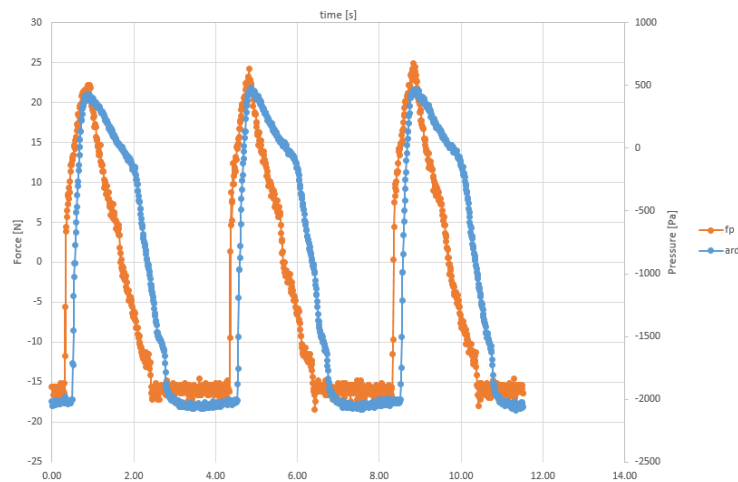


Figure 6.7: 0.25 Hz triangular wave, data from force plate (orange) and pressure sensor (blue)

6.6 Foot Testing

The next step in the experimental phase was to test the foot assembly on the lower leg test bench, designed in the DLS lab by Dr. Matteo Villa and used to test the new ISAs from Moog. In order to measure data from the force plate by using the test bench, wooden blocks (later metal), were bought by the student and fixed underneath the force plate's mounting frames by using screws. The height of the blocks was accurately measured before fixing them, to avoid errors in the read deriving from unevenly applied load. The first batch of tests was performed in conjunction with supervisor Dr. Victor Barasuol, aiming to assess the dynamic behavior of the sensor at varying loads applied, by keeping a constant frequency of swing. Unfortunately, the results were affected by the noise coming from the grounding issue described in the subsection above, therefore post-processing of the data had to be performed by using the moving average techniques, thus affecting the obtained results. Despite the failure, it was nonetheless a good starting point to become confident with the functionalities provided by the ISA through the CANOpen software interface, and the following experiments were carried out. The next batch of experiments was carried out to assess the effect of varying frequency of swing on the sensor's read, to assess if the gain, defined as Pressure/Force (Pa/N) was consistent. Below are reported graphs elaborated through Excel depicting the results obtained in this batch of experiments. The data they represent was elaborated through Matlab, to get results regarding the response time and the gain.

The results obtained in this experimental phase are summarized in the table 6.1:

6.6 Foot Testing

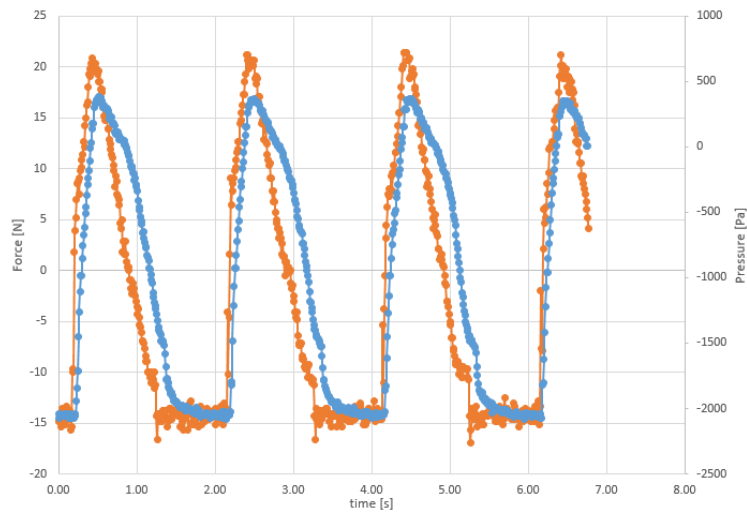


Figure 6.8: 0.50 Hz triangular wave, data from force plate (orange) and pressure sensor (blue)

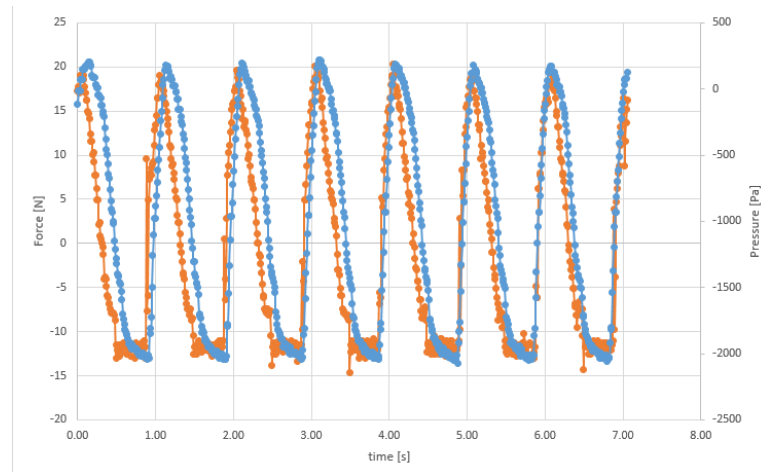


Figure 6.9: 1.00 Hz triangular wave, data from force plate (orange) and pressure sensor (blue)

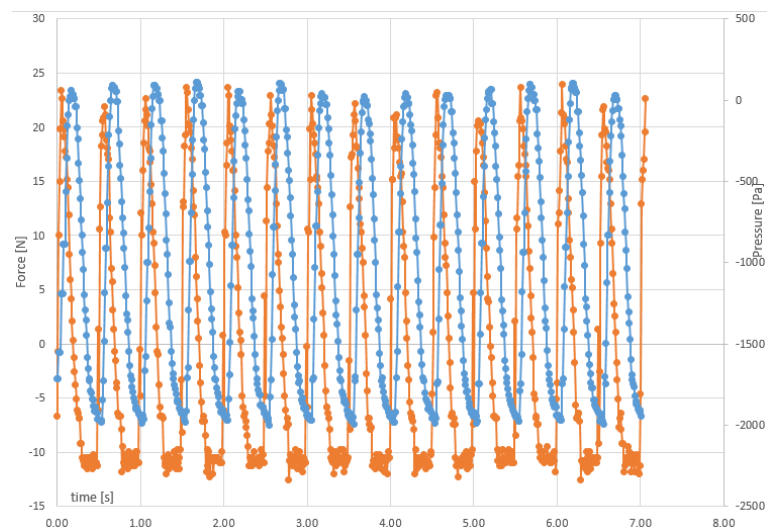


Figure 6.10: 2.00 Hz triangular wave, data from force plate (orange) and pressure sensor (blue)

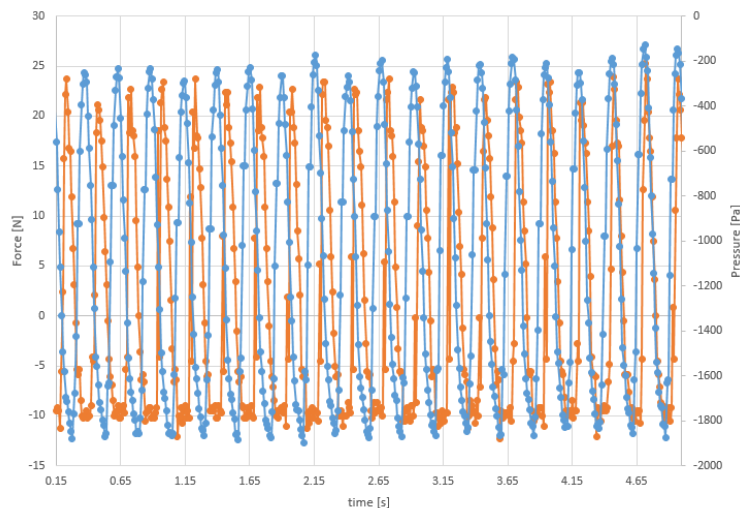


Figure 6.11: 5.00 Hz triangular wave, data from force plate (orange) and pressure sensor (blue)

Frequency	0.25 Hz	0.50 Hz	1.00 Hz	2.00 Hz	5.00 Hz
Gain [Pa/N]	59.2	64.4	65.5	57.8	47.1
Δt [ms]	60	50	60	64	72

Table 6.1: Experimental results: response time and gain

Through the analysis of these results, it was concluded that the sensor gain, which is critical in order to estimate the contact force resultant, is more or less consistent, with a computed deviation of $\pm 5\%$ on the average at frequencies up to 2 Hz, which is the frequency at which each leg swings during trotting locomotion. The drift is more evident at 5 Hz.

6.7 Vibration Effect on Sensor

The goal of this batch of experiments was to prove that the sensor is unaffected by high frequency vibration. This was necessary since one of the reasons why the current contact sensing methodology, which we recall is based on estimation, is not effective enough as it is prone to return false positives during the swing phase, due to the inertia of the leg and the foot. In particular, this effect is caused by the acceleration of the lower leg and inertia read through load cells included in the HAA and HFE transmission. For this batch of experiments no load was applied to the foot, as the swinging was performed mid air. Therefore, the results shown are only related to the pressure sensor. If the ΔP is below the one required for the contact sensing trigger, it will be proven that the sensor is unaffected by vibration. Figure 6.12 is a photo taken during this phase of experiments, to show the prototype in action and the test bench used.

6.7 Vibration Effect on Sensor

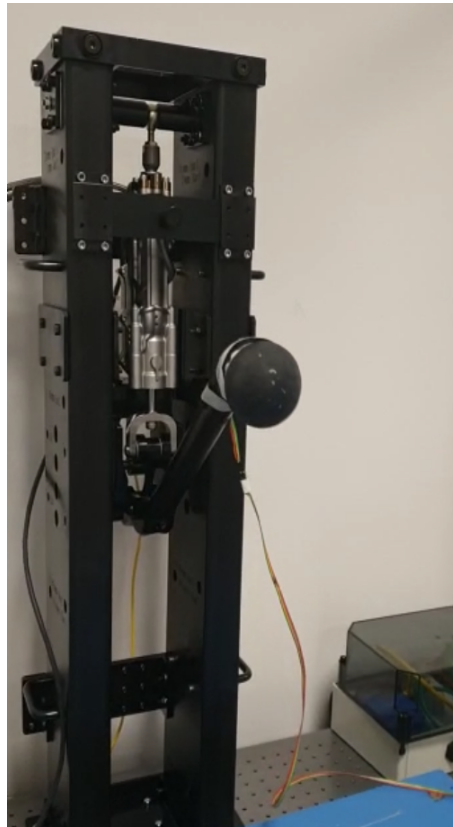


Figure 6.12: Experimental setup

Frequency	10 Hz	20 Hz	50 Hz	100 Hz
ΔP [Pa]	103	115	89	89

Table 6.2: Experimental results: vibration effect on pressure reading.

In Figure 6.13, it is shown the data obtained through the experiment as explained in this section. The data was then analyzed, the results of this are reported in Table 6.2.

Recalling that the requested trigger force is 25N and considering a gain (as computed in the preceding experiment) of 62 Pa/N , the trigger ΔP sits at around 1.5 kPa, ~ 13 times higher than the highest ΔP computed in this experiment, thus proving that the sensor is unaffected by high frequency swings and vibration.

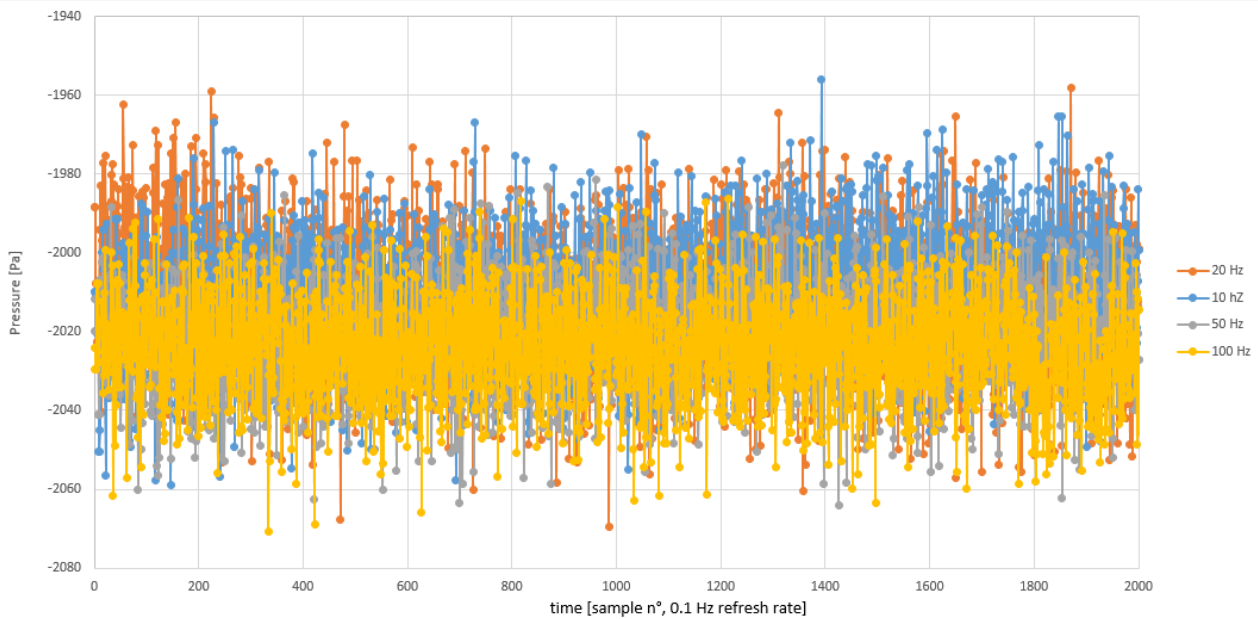


Figure 6.13: Raw data from pressure sensor at high frequency vibrations

6.8 Stress Test

In order to evaluate the performance of the prototype during prolonged use, it was setup a basic stress test. Data was collected from the pressure sensor at the beginning of the test, and at the end. In order to provide meaningful data, the leg was left swinging with a high load applied ($\sim 150\text{N}$) for about one hour. It is to be noted that the load was not higher not to risk breakage of the prototype, which we recall in this phase of experiments comprises an ABS internal structure which also interfaces with the screw of the foot through a brass insert. Once the metal prototype will be finalized and produced, higher loads will be applied and the performance will be tested again. The main concern, which was refuted through this experiment, was the presence of a drift in the pressure readings after a prolonged cycle of trotting, due to internal heating of the air constantly being compressed and expanded, and frictional contact at the rubber and pin interface.

Figure 6.14 reports the reading from the sensor at the beginning, and at the end of the experiment. It was also measured the force applied through the force plate to ensure a consistent gain. The blue line represents the pressure reading at the beginning of the experiment, whereas the orange line represents the pressure reading after 1 hour of swinging. It can be easily deduced that the sensor was unaffected and survived the experiment, the only appreciable change in behaviour being during the non-contact phase, identified in the trough of the sinusoidal wave.

6.8 Stress Test

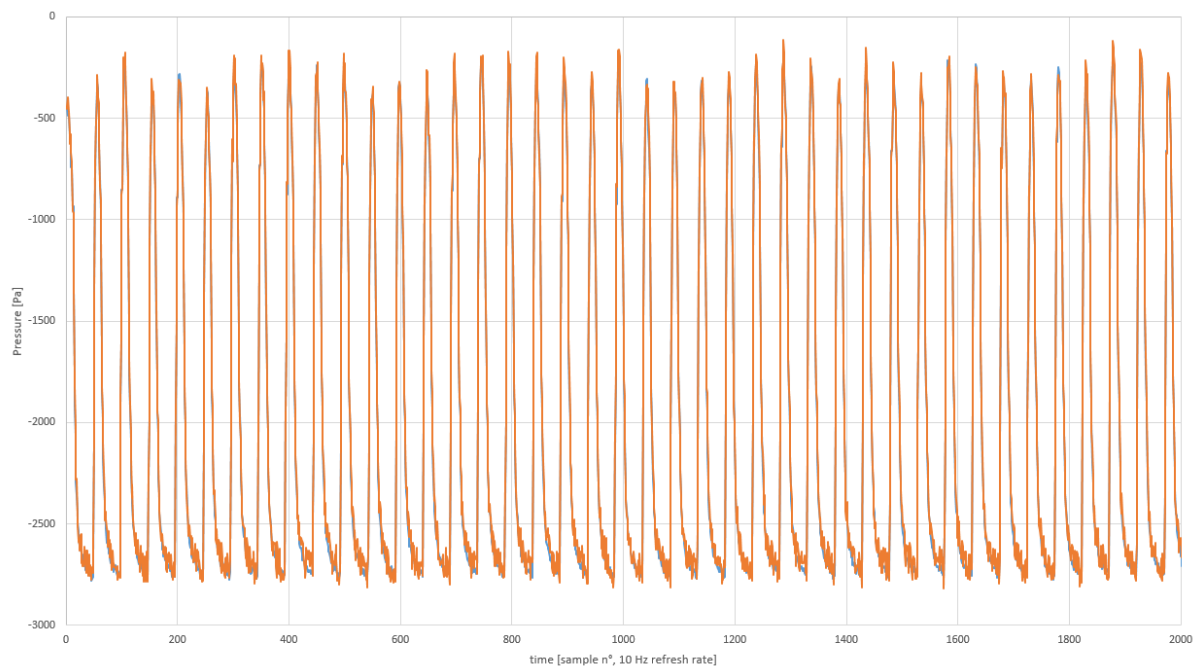


Figure 6.14: Stress test results, in blue beginning, in orange after one hour. Graphs superimposed a posteriori

This behaviour will be further explored once the aluminum prototype will be ready.

There are still many experiments to be performed on the new foot of the robot HyQReal before it can be used as the version consistently implemented in the robot, such as experiments performed on the robot itself with uneven terrains, and this will be assessed in future works.

Conclusions and Future Works

7.1 Conclusions

In the context of this thesis, it was presented an alternative design for the lower leg and foot of the robot HyQReal.

It was discussed which are the most promising sensor solutions found in the literature in order to add the capability to detect ground contact, and it was followed a rigorous rationale to make an educated choice. The proposed foot was then prototyped after numerous iterations of design and numerical analyses, as presented in Chapter 4, and tested through a series of experiments reported in Chapter 6. Parallely, a script was developed with the goal of optimizing the geometry of the shin of a quadruped robot for the specific application of stairs climbing, as presented in Chapter 5. It was proved, as reported in Chapter 6, that the proposed design would improve the ground detection capabilities of the robot HyQReal by lowering the threshold of contact sensing from 50 N to 10 N, but the durability, although tested on a fixed test bench, has to be furthered on the robot itself. It was also theoretically proved, as reported at the end of Chapter 5, that the new proposed shape of the lower leg, while respecting the geometric and kinematic limits proper of the robot HyQReal, would improve the reachability of the leg by 225% when going down stairs.

7.2 Future Works

There is much work and research to be done before considering this project closed. Starting from the prototyping, the experiments showed in the last chapter shall be repeated with a metal core, to allow reaching higher loads and removing the possibility (even though minimal) of backlash of coming from the interface between the screw connecting the toe to the foot, and the cap. Further investigation must also assess the effect of pressure waves propagating through an inlet, and it would also be advisable to investigate the possibility of a longer tube, to allow positioning the sensor further up inside the leg, to reduce the overall inertia and to protect the sensor itself from high impact loads which are a common occurrence at the foot level. Therefore experiments must be carried out to assess the durability of the design in an unstructured environment, on the robot itself. Furthermore, it must be assessed in a more rigorous way the drift from zero of the pressure sensor that occurs at each start-up, due mainly to atmospheric conditions, and strategies must be developed to correct this error each time. The communication interface of the sensor is the I^2C , a standard in the field, but the physical wiring to the communication hub, called T-REU and located within the ISA, has to be assessed as well.

Much of the work done on redesigning the lower leg is just theoretical up to now, but the results are valid, therefore the next step in the design will be to use the results obtained through the code optimizing the shape of the lower leg to design the new shin of the robot HyQReal. For what regards the materials used and the physical construction, the choice will likely be still to use aerospace-grade aluminum for the final product, as it provides excellent mechanical properties while keeping a low weight.

Regarding the future of the project, the idea would be to fuse the design of the foot and the results obtained and shown in Chapter 5 regarding the shin. Having a single piece configuration would decrease the complexity of the system, reducing the number of components, and increase the stiffness of the structure, by removing mechanical interfaces. At the end of Chapter 4, it was reported an alternative design for the new foot of the robot HyQReal. This alternative design would provide advantages, compared to the current proposal, both in terms of stiffness and durability, providing a good resistance to shear loads and less volume deformation required to trigger the contact. A prototype of this design would require some additional refinement, which is beyond the scope of the work presented in the context of this thesis, but would nonetheless be interesting to be investigated in the future, if the durability of the proposed design will result unreliable after the experiments on the robot will be carried out.

References

- [1] C. Semini, V. Barasuol, M. Focchi, C. Boelens, M. Emara, S. Casella, O. Villarreal, R. Orsolino, G. Fink, S. Fahmi *et al.*, “Brief introduction to the quadruped robot hyqreal,” *Istituto di Robotica e Macchine Intelligenti (I-RIM)*, 2019.
- [2] Y. Zhong, R. Wang, H. Feng, and Y. Chen, “Analysis and research of quadruped robot’s legs: A comprehensive review,” *International Journal of Advanced Robotic Systems*, vol. 16, no. 3, p. 1729881419844148, 2019. [Online]. Available: <https://doi.org/10.1177/1729881419844148>
- [3] C. Semini, N. G. Tsagarakis, E. Guglielmino, M. Focchi, F. Cannella, and D. G. Caldwell, “Design of hyq—a hydraulically and electrically actuated quadruped robot,” *Proceedings of the Institution of Mechanical Engineers, Part I: Journal of Systems and Control Engineering*, vol. 225, no. 6, pp. 831–849, 2011.
- [4] T. Boaventura, J. Buchli, C. Semini, and D. Caldwell, “Model-based hydraulic impedance control for dynamic robots,” *IEEE Transactions on Robotics*, vol. 31, pp. 1–13, 11 2015.
- [5] C. Semini, J. Goldsmith, B. U. Rehman, M. Frigerio, V. Barasuol, M. Focchi, and D. G. Caldwell, “Design overview of the hydraulic quadruped robots,” in *The fourteenth Scandinavian international conference on fluid power*. sn, 2015, pp. 20–22.
- [6] B. Siciliano and O. Khatib, *Springer Handbook of Robotics*, ser. Springer Handbook of Robotics. Springer Berlin Heidelberg, 2008. [Online]. Available: <https://books.google.it/books?id=Xpgi5gSuBxsC>
- [7] “Pressure measurement techniques: an overview,” <https://www.ni.com/it-it/innovations/white-papers/11/pressure-measurement-overview.html>, /.
- [8] “Pressure measurement techniques: an overview,” <https://sensing.honeywell.com/white-paper-effectivelyusingpressureloadandtorquesensorswithtodaydataacquisitionssystems-008883-2-en.pdf>, /.
- [9] “Pressure measurement techniques: an overview,” <https://www.fierceelectronics.com/components/pressure-measurement-principles-and-practice/>, /.
- [10] P. Biswal and P. K. Mohanty, “Development of quadruped walking robots: A review,” *Ain Shams Engineering Journal*, vol. 12, no. 2, pp. 2017–2031, 2021. [Online]. Available: <https://www.sciencedirect.com/science/article/pii/S2090447920302501>
- [11] “Hyq robot introduction,” https://www.youtube.com/watch?v=wPxXwYgZmd8&ab_channel=DynamicLeggedSystemslab, /.
- [12] “Isa description,” <https://www.moog.com/content/dam/moog/literature/ICD/Moog-Microhydraulics-Integrated-Smart-Actuator-Datsheet-en.pdf>, /.
- [13] Y. Kim, J. Kim, H. S. Kim, and T. Seo, “Curved-spoke tri-wheel mechanism for fast stair-climbing,” *IEEE Access*, vol. 7, pp. 173 766–173 773, 2019.
- [14] U. Saranlı, M. Buehler, and D. E. Koditschek, “Rhex: A simple and highly mobile hexapod robot,” *The International Journal of Robotics Research*, vol. 20, no. 7, pp. 616–631, 2001.
- [15] B. M. Yamauchi, “Packbot: a versatile platform for military robotics,” in *Unmanned ground vehicle technology VI*, vol. 5422. International Society for Optics and Photonics, 2004, pp. 228–237.
- [16] B. Seo, H. Kim, M. Kim, K. Jeong, and T. Seo, “Flipbot: a new field robotic platform for fast stair climbing,” *International Journal of Precision Engineering and Manufacturing*, vol. 14, no. 11, pp. 1909–1914, 2013.
- [17] D. Choi, Y. Kim, S. Jung, J. Kim, and H. S. Kim, “A new mobile platform (rhymo) for smooth movement on rugged terrain,” *IEEE/ASME Transactions on Mechatronics*, vol. 21, no. 3, pp. 1303–1314, 2016.

- [18] S. D. Herbert, A. Drenner, and N. Papanikolopoulos, “Loper: A quadruped-hybrid stair climbing robot,” in *2008 IEEE International Conference on Robotics and Automation*. IEEE, 2008, pp. 799–804.
- [19] “Ur5 robot, by universal robots,” <https://www.universal-robots.com/products/ur5-robot/>, /.
- [20] P. Gonzalez de Santos, E. Garcia, and J. Estremera, “The silo4 walking robot,” *Quadrupedal Locomotion: An Introduction to the Control of Four-legged Robots*, pp. 231–243, 2006.
- [21] “Boston dynamics’ spot robot,” <https://www.bostondynamics.com/products/spot/>, /.
- [22] “Anymal c from anybotics,” <https://www.anybotics.com/the-next-step-in-robotic-industrial-inspection/>, /.
- [23] B. Gamus and Y. Or, “Analysis of dynamic bipedal robot walking with stick-slip transitions,” in *2013 IEEE International Conference on Robotics and Automation*. IEEE, 2013, pp. 3348–3355.
- [24] P. Sardain and G. Bessonnet, “Forces acting on a biped robot. center of pressure-zero moment point,” *IEEE Transactions on Systems, Man, and Cybernetics-Part A: Systems and Humans*, vol. 34, no. 5, pp. 630–637, 2004.
- [25] S. Caron and Q.-C. Pham, “When to make a step? tackling the timing problem in multi-contact locomotion by topp-mpc,” in *2017 IEEE-RAS 17th International Conference on Humanoid Robotics (Humanoids)*. IEEE, 2017, pp. 522–528.
- [26] B. Brogliato and B. Brogliato, *Nonsmooth mechanics*. Springer, 1999.
- [27] C. Semini and P.-B. Wieber, “Legged Robots,” in *Encyclopedia of Robotics*. Springer, 2020, pp. 1–11. [Online]. Available: <https://hal.archives-ouvertes.fr/hal-02461604>
- [28] A. Ji, Z. Dai, and L. Zhou, “Research development of bio-inspired robotics,” *Robot*, vol. 27, no. 3, pp. 284–288, 2005.
- [29] M. Tan and S. Wang, “Research progress on robotics,” *Acta Automatica Sinica*, vol. 39, no. 7, pp. 963–972, 2013.
- [30] Y. Zhong, R. Wang, H. Feng, and Y. Chen, “Analysis and research of quadruped robot’s legs: a comprehensive review,” *International Journal of Advanced Robotic Systems*, vol. 16, no. 3, p. 1729881419844148, 2019.
- [31] “Boston dynamics website,” <https://www.bostondynamics.com/>, /.
- [32] J.-d. Wang, K.-y. Lu, S.-f. Xu, and Y.-y. Lei, “Research situation and prospect on quadruped walking robot,” *Manufacturing automation*, vol. 2, no. 1, pp. 4–6, 2009.
- [33] S. Seok, A. Wang, M. Y. Chuah, D. Otten, J. Lang, and S. Kim, “Design principles for highly efficient quadrupeds and implementation on the mit cheetah robot,” in *2013 IEEE International Conference on Robotics and Automation*. IEEE, 2013, pp. 3307–3312.
- [34] J. E. McKenzie, “Design of robotic quadruped legs,” Ph.D. dissertation, Massachusetts Institute of Technology, 2012.
- [35] M. H. Raibert, *Legged robots that balance*. MIT press, 1986.
- [36] M. Ahmadi and M. Buehler, “Preliminary experiments with an actively tuned passive dynamic running robot,” in *Experimental Robotics V*. Springer, 1998, pp. 312–324.
- [37] I. Poulakakis, J. A. Smith, and M. Buehler, “Modeling and experiments of untethered quadrupedal running with a bounding gait: The scout ii robot,” *The International Journal of Robotics Research*, vol. 24, no. 4, pp. 239–256, 2005.
- [38] M. H. Raibert, H. B. Brown Jr, M. Chepponis, E. Hastings, S. E. Shreve, and F. C. Wimberly, “Dynamically stable legged locomotion research,” 1981.
- [39] S. Kitano, S. Hirose, A. Horigome, and G. Endo, “Titan-xiii: sprawling-type quadruped robot with ability of fast and energy-efficient walking,” *Robomech Journal*, vol. 3, no. 1, pp. 1–16, 2016.
- [40] E. Garcia, J. C. Arevalo, G. Muñoz, and P. Gonzalez-de Santos, “Combining series elastic actuation and magneto-rheological damping for the control of agile locomotion,” *Robotics and Autonomous Systems*, vol. 59, no. 10, pp. 827–839, 2011.
- [41] E. Garcia, J. C. Arevalo, G. Munoz, and P. Gonzalez-de Santos, “On the biomimetic design of agile-robot legs,” *Sensors*, vol. 11, no. 12, pp. 11 305–11 334, 2011.
- [42] K. Gudmundsson, F. Jonsdottir, and F. Thorsteinsson, “A geometrical optimization of a magneto-rheological rotary brake in a prosthetic knee,” *Smart Materials and Structures*, vol. 19, p. 035023, 02 2010.
- [43] M. Focchi, A. del Prete, I. Havoutis, R. Featherstone, D. G. Caldwell, and C. Semini, “Ground reaction forces control for torque-controlled quadruped robots,” in *IEEE International Conference on Intelligent Robots and Systems: Workshop on Whole-Body Control for Robots in the Real World*, 2014.

-
- [44] G. Xin, H.-C. Lin, J. Smith, O. Cebe, and M. Mistry, "A model-based hierarchical controller for legged systems subject to external disturbances," 05 2018, pp. 4375–4382.
- [45] T. Poggio, "Marr's computational approach to vision," *Trends in neurosciences*, vol. 4, pp. 258–262, 1981.
- [46] S. Fahmi, C. Mastalli, M. Focchi, and C. Semini, "Passive whole-body control for quadruped robots: Experimental validation over challenging terrain," *IEEE Robotics and Automation Letters*, vol. 4, no. 3, pp. 2553–2560, 2019.
- [47] T. Barfoot, *State Estimation for Robotics*. Cambridge University Press, 2017. [Online]. Available: <https://books.google.it/books?id=2SstDwAAQBAJ>
- [48] V. Sharma and H. K. Verma, "Optimized fuzzy logic based framework for effort estimation in software development," *arXiv preprint arXiv:1004.3270*, 2010.
- [49] S. Fahmi, G. Fink, and C. Semini, "On state estimation for legged locomotion over soft terrain," *IEEE Sensors Letters*, vol. 5, no. 1, pp. 1–4, 2021.
- [50] C. E. Schroeder, D. A. Wilson, T. Radman, H. Scharfman, and P. Lakatos, "Dynamics of active sensing and perceptual selection," *Current opinion in neurobiology*, vol. 20, no. 2, pp. 172–176, 2010.
- [51] J. Casals-Terre and A. Shkel, "Dynamic analysis of a snap-action micromechanism," in *SENSORS, 2004 IEEE*. IEEE, 2004, pp. 1245–1248.
- [52] "Force Sensing Resistors overview, howpublished = <https://learn.adafruit.com/force-sensitive-resistor-fsr>, note = /."
- [53] "Optoforce sensor," <http://www.quadratec-ltd.co.uk/optoforce-force-sensing-systems.asp>, /.
- [54] "Hyqreal pulling an airplane," https://www.youtube.com/watch?v=pLsNs1ZS_TI, /.
- [55] R. Dang, L. Jiang, Q. Yao, P. Xu, Y. Jiang, and B. Su, "The research status on foot design and motion control of the legged robot in soft terrain," in *2019 IEEE International Conference on Unmanned Systems (ICUS)*, 2019, pp. 162–166.
- [56] Y. Nakasone, S. Yoshimoto, and T. Stolarski, "Chapter 2 - overview of ansys structure and visual capabilities," in *Engineering Analysis with ANSYS Software*, Y. Nakasone, S. Yoshimoto, and T. Stolarski, Eds. Oxford: Butterworth-Heinemann, 2006, pp. 37–50. [Online]. Available: <https://www.sciencedirect.com/science/article/pii/B9780750668750500326>
- [57] "Mpl3115a250 datasheet," https://www.distrelec.it/Web/Downloads/_t/ds/Freescale_MPL3115_eng.tds.pdf, /.
- [58] S. Hirose, E. Fukushima, R. Damoto, and H. Nakamoto, "Design of terrain adaptive versatile crawler vehicle helios-vi," in *Proceedings 2001 IEEE/RSJ International Conference on Intelligent Robots and Systems. Expanding the Societal Role of Robotics in the the Next Millennium (Cat. No.01CH37180)*, vol. 3, 2001, pp. 1540–1545 vol.3.
- [59] M. J. Lawn, T. Sakai, M. Kuroiwa, and T. Ishimatsu, "Development and practical application of a stair-climbing wheelchair in nagasaki," *Journal of HWRS-ERC*, vol. 2, no. 2, pp. 33–39, 2001.
- [60] S. Yu, T. Wang, X. Li, C. Yao, Z. Wang, and D. Zhi, "Configuration and tip-over stability analysis for stair-climbing of a new-style wheelchair robot," *2010 IEEE International Conference on Mechatronics and Automation*, pp. 1387–1392, 2010.
- [61] N. J. Baishya, B. Bhattacharya, H. Ogai, and K. Tatsumi, "Analysis and design of a minimalist step climbing robot," *Applied Sciences*, vol. 11, no. 15, 2021. [Online]. Available: <https://www.mdpi.com/2076-3417/11/15/7044>
- [62] Y. Zhu, Y. Fei, and H. Xu, "Stability analysis of a wheel-track-leg hybrid mobile robot," *Journal of Intelligent & Robotic Systems*, vol. 91, no. 3, pp. 515–528, 2018.
- [63] J. Yuan and S. Hirose, "Research on leg-wheel hybrid stair-climbing robot, zero carrier," in *2004 IEEE International Conference on Robotics and Biomimetics*. IEEE, 2004, pp. 654–659.
- [64] Y. Cao, K. Lu, X. Li, and Y. Zang, "Accurate numerical methods for computing 2d and 3d robot workspace," *International Journal of Advanced Robotic Systems*, vol. 8, no. 6, p. 76, 2011.
- [65] T. Koolen, S. Bertrand, G. Thomas, T. De Boer, T. Wu, J. Smith, J. Engelsberger, and J. Pratt, "Design of a momentum-based control framework and application to the humanoid robot atlas," *International Journal of Humanoid Robotics*, vol. 13, no. 01, p. 1650007, 2016.
- [66] C. D. Bellicoso, F. Jenelten, C. Gehring, and M. Hutter, "Dynamic locomotion through online nonlinear motion optimization for quadrupedal robots," *IEEE Robotics and Automation Letters*, vol. 3, no. 3, pp. 2261–2268, 2018.

- [67] V. Barasuol, G. Fink, M. Focchi, D. Caldwell, and C. Semini, “On the detection and localization of shin collisions and reactive actions in quadruped robots,” in *International Conference on Climbing and Walking Robots*, 2019.
- [68] A. Del Prete, F. Nori, G. Metta, and L. Natale, “Control of contact forces: the role of tactile feedback for contact localization,” 10 2012.
- [69] S. Ivaldi, M. Fumagalli, M. Randazzo, F. Nori, G. Metta, and G. Sandini, “Computing robot internal/external wrenches by means of inertial, tactile and f/t sensors: Theory and implementation on the icub,” in *2011 11th IEEE-RAS International Conference on Humanoid Robots*, 2011, pp. 521–528.
- [70] A. de Luca and R. Mattone, “Sensorless robot collision detection and hybrid force/motion control,” in *Proceedings of the 2005 IEEE International Conference on Robotics and Automation*, 2005, pp. 999–1004.
- [71] B. Siciliano, L. Sciavicco, L. Villani, and G. Oriolo, “Modelling, planning and control,” *Advanced Textbooks in Control and Signal Processing*. Springer,, 2009.